ESCUELA SUPERIOR POLITÉCNICA DEL LITORAL

FACULTAD DE INGENIERÍA MARÍTIMA CIENCIAS BIOLÓGICAS, OCEANOGRÁFICAS Y RECURSOS NATURALES

"GULF OF GUAYAQUIL TIDAL SIMULATION USING DELFT3D HYRODINAMIC MODEL DURING AN EL NIÑO EVENT AND NORMAL CONDITIONS"

CAPSTONE PROJECT REPORT

Prior to receiving the degree of:

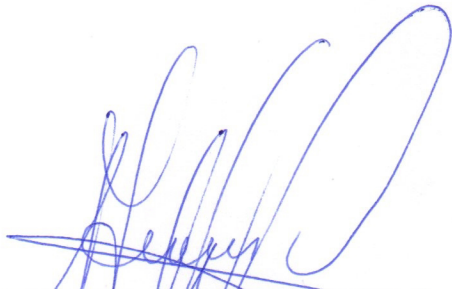## INGENIERA OCEÁNICA AMBIENTAL

MARÍA ESTHER ESPINOZA CELI

GUAYAQUIL – ECUADOR

YEAR: 2018

ACKNOWLEDGMENTS

EVALUATION COURT

Franklin Ormaza González, Ph.D
EVALUATOR TEACHER

Mercy Borbor Córdova, Ph.D.
ACADEMIC ADVISOR

EXPRESS STATEMENT

"The responsibility and authorship of the content of this degree work, corresponds exclusively to me; and I give my consent so that ESPOL can make public communication of this work with the goal to promote the consult, diffusion and public use of the intellectual production"

María Esther Espinoza Celi

SUMMARY

During an El Niño event higher tides than usual may occur in coastal areas such as the Gulf of Guayaquil, because of the rise in sea level produced in the Eastern Pacific by this climate phenomenon. To increase the knowledge about this effect in the Gulf, a tidal simulation was performed using the Delft3D hydrodynamic model, during the year 2015 of the most recent El Niño 2015-16 and during the year 2014 corresponding to a normal year. The simulated months were April (wet season) and June (dry season) for both years. In this way, it was possible to compare the tidal height in the Gulf during one year with El Niño conditions and one year with normal conditions.

The simulated area covered the outer estuary, from the Sprig of Santa Elena, to the areas of Estero Salado and north of Mondragon Island in the Guayas River corresponding to the inner estuary. The temporal resolution of the model was of results at intervals of 10 min and a spatial resolution in a range of 500 m -1 km in the inner Gulf and less than 4 km in the outer Gulf. The model was calibrated and validated with measured data from tide gauge stations of the Ecuadorian National Oceanographic Institute of Navy (INOCAR).

It was found that during El Niño in 2015, the tides were higher in the Gulf in April and June, both during the spring and neap tides dates analyzed, compared to the tidal height in 2014 with normal conditions. Additionally, a few results from another application of the Delft3D model were presented in terms of the magnitude of the current velocities in the study area. These last results also showed greater magnitudes of current velocity in the year 2015 of the El Niño 2015-16 event, in contrast to the velocities of the year 2014 corresponding to a normal year.

CONTENTS

INTRODUCTION

The El Niño 2015-2016 event has been cataloged as one of the strongest in recent decades. It is considered that this phenomenon is one of the most influential factors in natural climate variability [1]. Its effects occur globally, one of them is the rise in sea level in the Eastern Pacific [2] which can cause a tidal amplification producing higher tides than usual [3] in countries located in that area of the Pacific. When this occurs, the coasts of countries such as Ecuador may become vulnerable to severe erosion processes that affect tourist beaches, piers, ports and many coastal structures.

In Ecuador, the Gulf of Guayaquil is an area of great economic and tourist importance for the country, as well as home to several coastal populations that could be vulnerable to the effects of high tides during El Niño. In fact, it has already been reported by Deltares that sea level rise due to El Niño produces higher tides in cities such as Guayaquil. On the other hand, the characteristic morphology of the Gulf plays an important role in the tidal amplification, since in this type of ecosystem, due to the existence of narrow channels, the tide is amplified as it enters [4].

To study and comprehend more fully this effect produced in the Gulf due to a climatic event such as El Niño, the application of numerical models is very useful. Unlike satellite information that also allows the study of the ocean in different parts of the world, but has limitations regarding its temporal and spatial resolution [5], numerical models allow to provide and visualize information on variables such as water level in more detail in large inlets of water like the Gulf of Guayaquil.

In this context, it is important and necessary to generate more information and knowledge about the behavior of the tides in the Gulf during an El Niño event, especially during El Niño 2015-16 since it is the most recent and therefore not yet studied as past events. To study the tides during the El Niño 2015-16 event, the tides were simulated during the months of April and June of 2015 corresponding to El Niño conditions, and it was taken as reference the same periods of time of 2014 that presented normal conditions.

The simulation was carried out in two dimensions using the numerical model Delft3D through its hydrodynamic module FLOW. Therefore, it was possible to make comparisons between El Niño conditions and normal conditions in relation to the tidal height in the Gulf area. In this way, the general objective of this project is to perform a tidal simulation in the Gulf of Guayaquil during the El Niño 2015-16 event implementing the Delft3D-FLOW hydrodynamic model. Consequently, the following are proposed as specific objectives:

- Definition of the geographical system of analysis in the model creating the numerical grid, using the bathymetry and defining initial and boundary conditions.

- Calibration and validation of the model for water levels using tide gauge measurements to define the optimal Manning roughness coefficient and Eddy viscosity according to the geographical conditions of the system.

- Running of the model with the previously defined conditions and physical parameters to simulate tidal propagation in the Gulf for the periods of time to be studied.

Chapter 1 contains a literature review related to the tides in the Gulf of Guayaquil, as well as a description of the development of the El Niño 2015-16 event. A description of the relationship between El Niño and tidal amplification is included according to previous studies. Additionally, precipitation and flow conditions are detailed as reported by the National Institute of Meteorology and Hydrology (INAMHI) of Ecuador, during the periods of time to be studied. The methodology applied in the project related to the construction of the Delft3D-FLOW model is found in Chapter 2. Once the model is constructed, the calibration and validation process are detailed in Chapter 3. Finally, in Chapter 4 the results obtained from the simulation during El Niño conditions in 2015 and normal conditions in 2014 are analyzed.

CHAPTER 1

1. LITERATURE REVIEW

1.1. The Gulf of Guayaquil

1.1.1. General characteristics

The Gulf of Guayaquil is divided into two environments, internal and outer estuary [6], [7], [8]. The internal estuary is comprised of two ecosystems, the Guayas River and the Estero Salado, which are connected to each other by several channels, of which the Cascajal channel stands out as the largest. In addition, the Cascajal channel also connects the Morro and Jambeli channels, which surround the Puna Island as represented in figure 1.1 [6].

Unlike the Guayas River formed by the confluence of the Daule and Babahoyo Rivers, the Estero Salado whose length is approximately 70 km from the Morro channel to the inner estuary [9], does not receive important freshwater discharges [6] and is not influenced by the input of freshwater of the Guayas river [7]. In fact, it has been reported that the Guayas River covers 64% of the total basin drainage, thus being the main source of freshwater in the Gulf [7], [8].
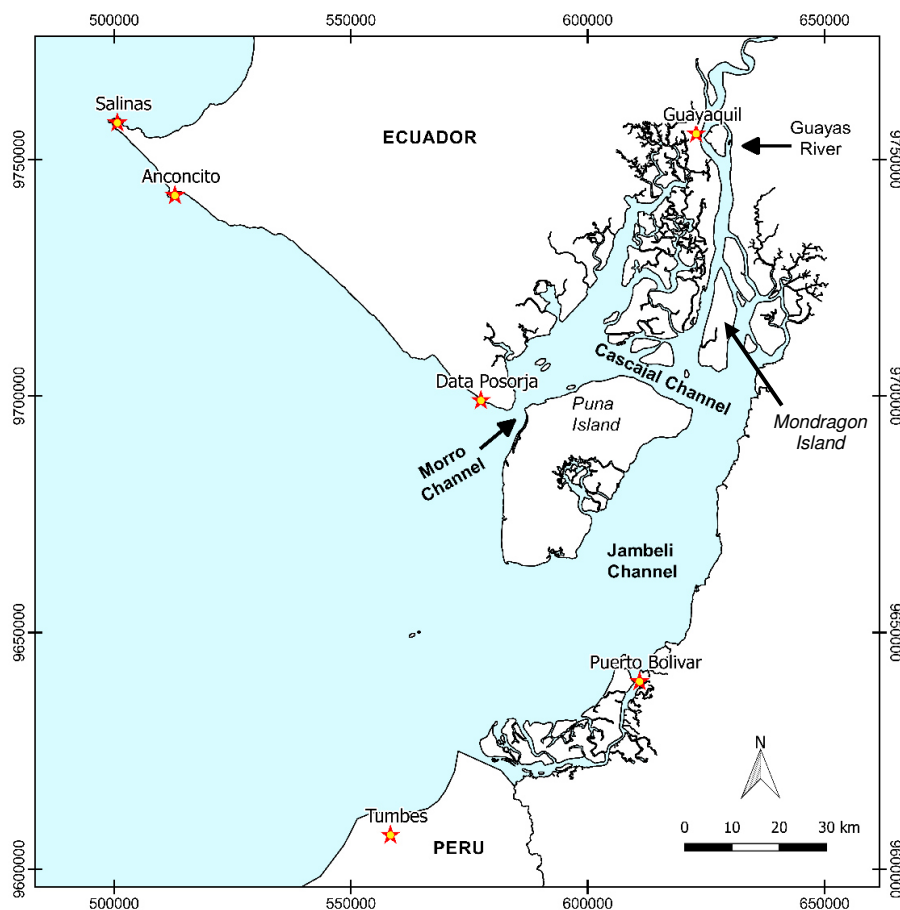

Figure 1.1.- Study area: Gulf of Guayaquil. Source: Author's elaboration.

1.1.2. Tides

Although the magnitude of the tides is influenced by the positions of the sun, the moon and the earth, on a small scale there are other factors that can significantly influence. For example, in bays and estuaries the intensity of tides may be higher due to its morphology. If there are narrow channels, the magnitude of tides may increase. The opposite happens in areas with shallow water or wide channels. In the same way, rivers with significant discharges, wind and weather patterns may affect tides intensifying or dissipating them [10].

Moreover, tides may have diurnal, semidiurnal or mixed patterns in different parts of the world. In Ecuador tides are semidiurnal, which means that two highs and two lows of the same height occur every day. These tidal patterns have an estimated period of 12 hours. In the Gulf of Guayaquil, the tidal wave is aligned according to its morphology and enters from the southwest. The tide reaches the Cascajal area first through the Morro channel and then through the Jambeli channel since its length is greater [11].

In addition, according to [7] when the tides enter along the entrance of the Gulf they are in phase, however, while they are moving towards the interior a lag due to friction is generated, which is 4h18min with respect to the high tide between Salinas or Talara (Perú) and Guayaquil. In general, towards the outer zone of the Gulf the tides have 1.8 m, value that increases towards its interior near the city of Guayaquil to approximately between 3-5 m [7], [12].

1.2. El Niño 2015-2016

El Niño events are periods of anomalous climatic conditions in the tropical Pacific which causes a weakening of the trade winds [1]. These events are caused by an alteration of the ocean-atmosphere system [13] and impact several countries around the world. El Niño 2015-16 has been cataloged by the World Meteorological Organization (WMO) as one of the strongest since 1950, along with the events of 1982-83 and 1997-98. This event began its development in 2015 and began to weaken since March 2016 [1].

Between November and December 2015, the first high peaks of anomalies of Sea Surface Temperature (SST) were presented. However, signs of an El Niño event appeared since 2014 when westerly wind anomalies were already observed and positive anomalies of SST by the end of the year were up to 2° C in the Equatorial Pacific [1]. CIIFEN in [1], reports that in March 2015 the first Kelvin wave occurred and by the end of April it arrived at the west coast of South America due to westerly winds anomalies of up to 16 m/s.

The arrival of Kelvin waves increases temperature and water level in the Western Pacific. More Kelvin pulses occurred in May, July, August, October and November 2015. During April 2015 positive SST anomalies in the Equatorial Eastern Pacific reached 3°C. Between November and December 2015 and January 2016 El Niño reached its maximum intensity. Finally, CIIFEN indicates that in June 2016, the neutral phase of the ENSO began in the tropical Pacific [1].

In Ecuador, precipitations during El Niño 2015-16 were not as intense compared to El Niño 1997 and 1982 as observed by the National Institute of Meteorology and Hydrology (INAMHI). It was in the provinces of Esmeraldas and north of Manabi where 53% of the floods occurred during the first quarter of 2016, being the most affected provinces during this phenomenon. On the other hand, Los Rios and Guayas provinces constituted 20%, where in the latter more than 3500 people were affected by El Niño [14].
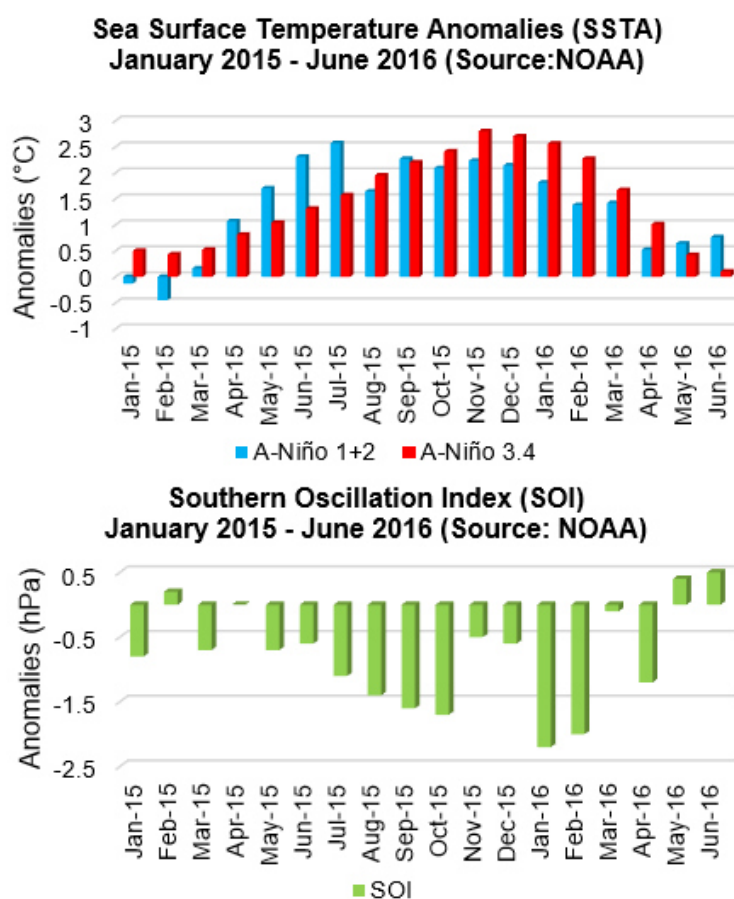

Figure 1.2.- Sea Surface Temperature Anomalies in the Niño 1+2 and Niño 3.4 regions and Southern Oscillation Index-SOI in the Tropical Pacific in 2015. Source: Author's elaboration based on data from the National Oceanic and Atmospheric Administration-NOAA [15]

As seen in figure 1.2, between November and December 2015 until January 2016, the largest positive TSS anomalies were registered in the Niño 3.4 region, which coincides with the period in which El Niño had its greatest intensity. While, in the Niño 1+2 region, the highest positive anomalies occurred between June and July 2015. In both regions the anomalies began to decrease until June 2016 when the neutral phase of the ENSO began as indicated by CIIFEN in [1]. The South Oscillation Index (IOS) shows that there were negative anomalies in January and March 2015 and then from May 2015 to April 2016, reaching anomalies of up to -2 hPa and -2.2 hPa in the first two months of 2016.

1.3. Influence of El Niño events in sea level rise

Sea level rise is an important impact of El Niño events. As the trade winds weaken and the westerly winds intensify, Kelvin waves are generated and move from the Western Pacific to the Eastern Pacific [1], [13]. Therefore, during an El Niño event, the sea level in the Eastern Pacific Ocean increases. It is important to mention that the amplitude of Kelvin waves will not only influence the elevation of the sea level but also currents[2]. For example, during the El Niño 1982-1983 the sea level intensified from April 1982 to January 1983, possibly as a consequence of the westerly winds [2]. The first peak of 30 cm above average occurred at La Libertad in January 1983 due to the arrival of a large Kelvin wave [16].

On the coasts of California, high sea levels were recorded during El Niño 2015-16. In October 2015 tide gauge records indicated elevations between 15-23 cm above normal. The warming of the waters in the ocean during El Niño produces a sea level rise of a few inches. But added to this, sea levels intensify when the winter season arrives. For example, during the winters of the El Niño events of 1982-83 and 1997-98 the sea level increased between 15-25 cm in San Francisco and La Jolla [3].

1.4. The influence of sea level rise on the amplification of tides

In the Guayas estuary the tides are amplified as the tidal wave moves towards the interior of the system, this is due to its morphology. For example, between Guayaquil and Puerto Bolivar the tides are higher in Guayaquil because this city is located more internally in the estuary. The freshwater discharges of rivers to the Gulf changes between the wet and dry season, being greater during wet season when abundant precipitations occur. These two factors cause an elevation of the sea level in the Gulf that will be more evident during spring tides than during neap tides [4].

The amplification of tides will be much greater if El Niño conditions are present, since the sea level can rise to 30 cm [4]. Coastal cities can suffer severe impacts when high sea levels coincide with high tides. When El Niño conditions exist, the tides are amplified,

generating erosion on the coast and affecting the infrastructure [3]. Deltares has reported that with the application of the Delft3D-FM model, it has been observed that the rise in sea level causes higher tides in cities such as Guayaquil and that the tidal amplitude intensifies more when the tide rises than when it decreases (Figura 1.3) [4].
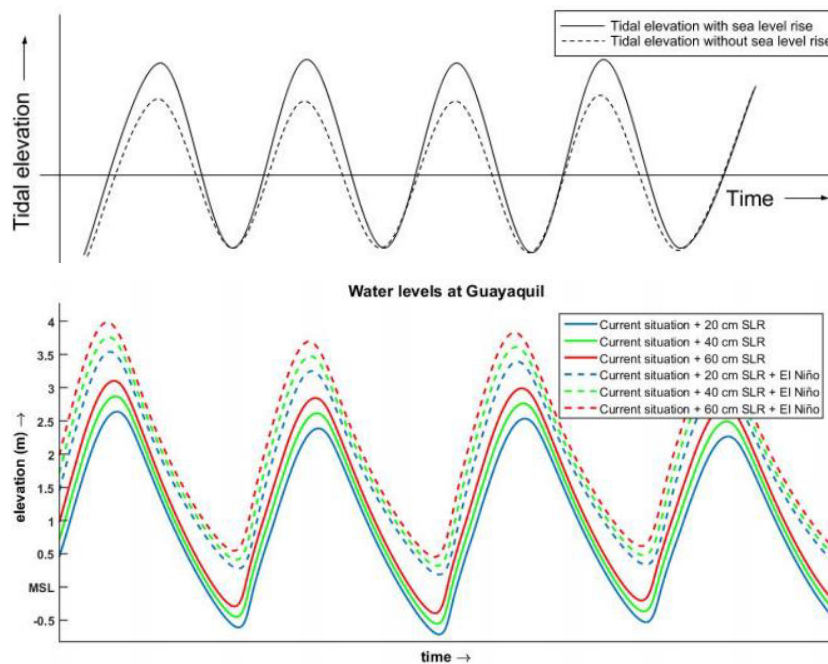
Figure 1.3.- Influence of El Niño in water levels of Guayaquil during spring tides and considering river discharges. Source: Deltares 2016 [15].

1.5. Precipitations

1.5.1. Precipitations in 2015

According to the National Institute of Meteorology and Hydrology (INAMHI) of Ecuador, in its Annual Climatological Bulletin of 2015 the annual rainfall recorded in the littoral region showed increases in the north of Ecuador and decreases in the south. For example, in the Guayaquil-Airport pluviometric station, an accumulated annual precipitation of 966.6 mm was recorded (Figure 1.4), which corresponds to a 25% decrease in the normal annual precipitation of 1285.6 mm. In other cities such as Milagro, Babahoyo and Zaruma there were also decreases in annual accumulated precipitation during 2015 [17].

Additionally, as indicated in figure 1.5, of the pluviometric stations located in the littoral region Guayaquil-Aeropuerto is one of those that recorded the lowest amount of days (90 days) in which there was precipitation in 2015 along with the stations of Chone (89 days) and Babahoyo (76 days). While, in cities such as: Esmeraldas, Portoviejo, Pichilingue and Santa Rosa, the number of days in the year that there was precipitation exceeds the amount of 100 [17]. On the other hand, INAMHI reported that the highest

precipitation recorded in 24 hours in 2015 was in the month of April at stations Guayaquil-Aeropuerto (112 mm), Chone (51.8 mm) and Babahoyo (142.6 mm). In general, in the coastal region precipitation was more frequent in April and March 2015.
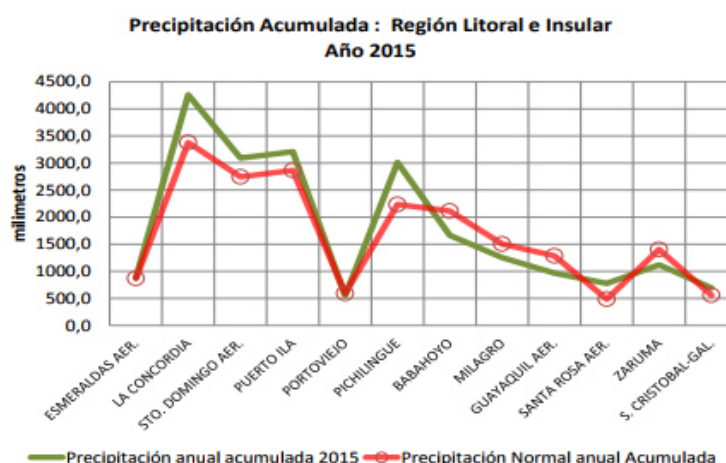
Figure 1.4.- Cumulative rainfall in 2015 in the Litoral and Insular Region of Ecuador. Source: INAMHI [16].
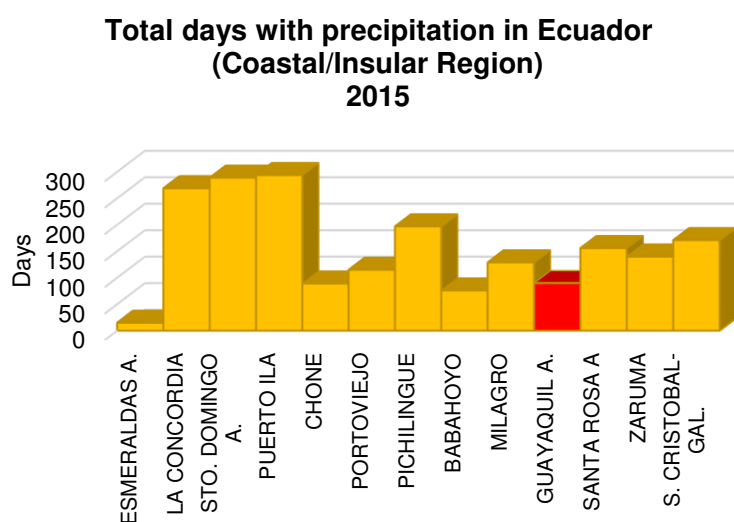
Figure 1.5.- Total days with precipitation in the Coastal/Insular region of Ecuador during 2015. Source: Author's elaboration based on INAMHI in [16].

April 2015

In April 2015, the precipitation reported in the city of Guayaquil at the beginning of the month was weak and intensified until the end of the month. In general, in all pluviometric stations of the city, accumulated precipitation in April was higher than the historical average of the month (Figure 1.6). As a result, it was considered a month with precipitation in a "very normal" range at the Guayaquil-Aeropuerto station and "above

normal" at the Guayaquil-INOCAR station, according to the classification by quintiles of INAMHI [18].

Figure 1.6.- Precipitation by stations in Guayaquil during the month of April 2015. Source: INAMHI [17].

- April 18, 2015

  Weak precipitation was recorded, with a maximum of 0.5 mm at the Duran station [19].

- April 25, 2015

  Weak precipitation was recorded, with a maximum of 0.1 mm at the Duran and Ciudadela Universitaria (UG) stations [20].

June 2015

In June 2015 the precipitation was of variable intensity the first days of the month and during the course of the month they went from weak to nil. In general, during this month all the stations located in Guayaquil recorded precipitations with values higher than the historical average of the month (Figure 1.6). Both in the Guayaquil-Aeropuerto station and in the Guayaquil-INOCAR station, the precipitation in June 2015 was in a "very normal" range, according to the classification by quintiles of the INAMHI [21].

Figure 1.7.- Precipitation by stations in Guayaquil during the month of June 2015. Source: INAMHI [18].

- June 2, 2015

  Weak precipitation was recorded, with a maximum of 4.9 mm at Ciudadela Universitaria (UG) station [22].

- June 24, 2015

  No precipitation was recorded in the city [23].

1.5.2. Precipitations in 2014

April 2014

In April 2014, weak precipitation was recorded, therefore, the accumulated precipitation was below the historical average for this month (Figure 1.8). In the Guayaquil-Airport station, precipitation in April 2014 was found in a "low-normal" range and in the Guayaquil-INOCAR station in a "normal" range, according to the classification by quintiles of INAMHI [24].
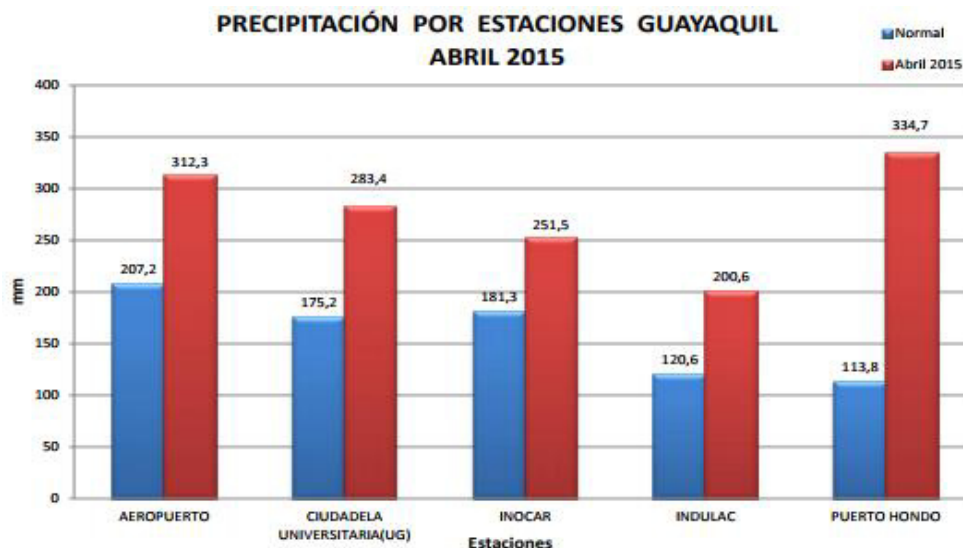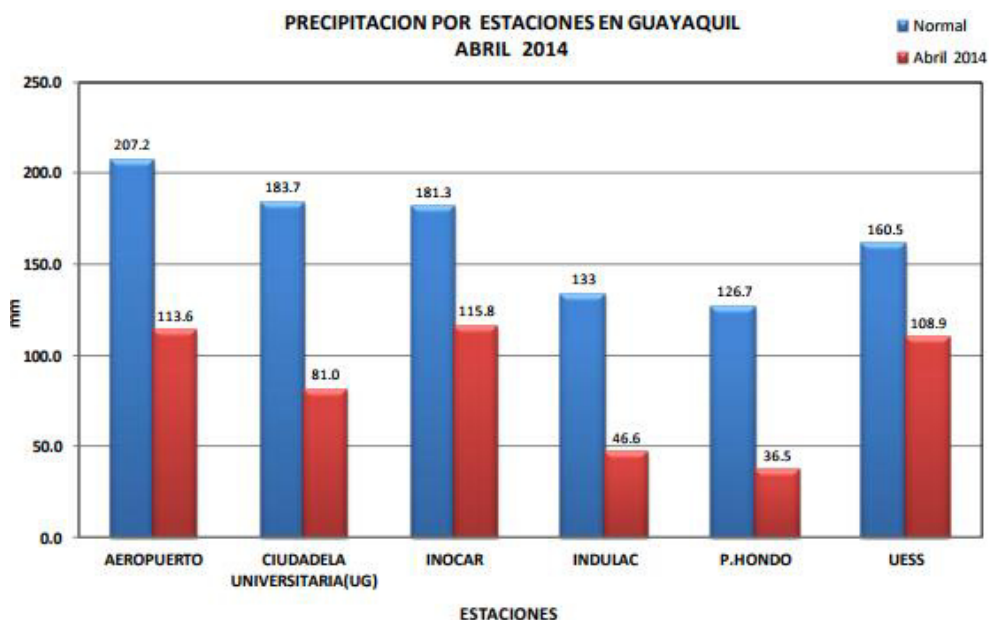
Figure 1.8.- Precipitation by stations in Guayaquil during the month of April 2014. Source: INAMHI [17].

- April 7, 2014

  Precipitation of weak to moderate intensity was recorded in the city. The maximum recorded precipitation was at the INOCAR station with 12.7 mm [25].

- Abril 29, 2014

  Isolated drizzles were recorded, with a maximum of 0.2 mm at the Puerto Hondo station [26].

June 2014

In June 2014, precipitation registered in the city of Guayaquil was weak throughout the month except for day 3. However, precipitation values were recorded above the historical median (Figure 1.9). In the Guayaquil-Aeropuerto station and in the Guayaquil-INOCAR station, precipitation in June 2014 was found in a range "above normal", according to the classification by quintiles of INAMHI [27].
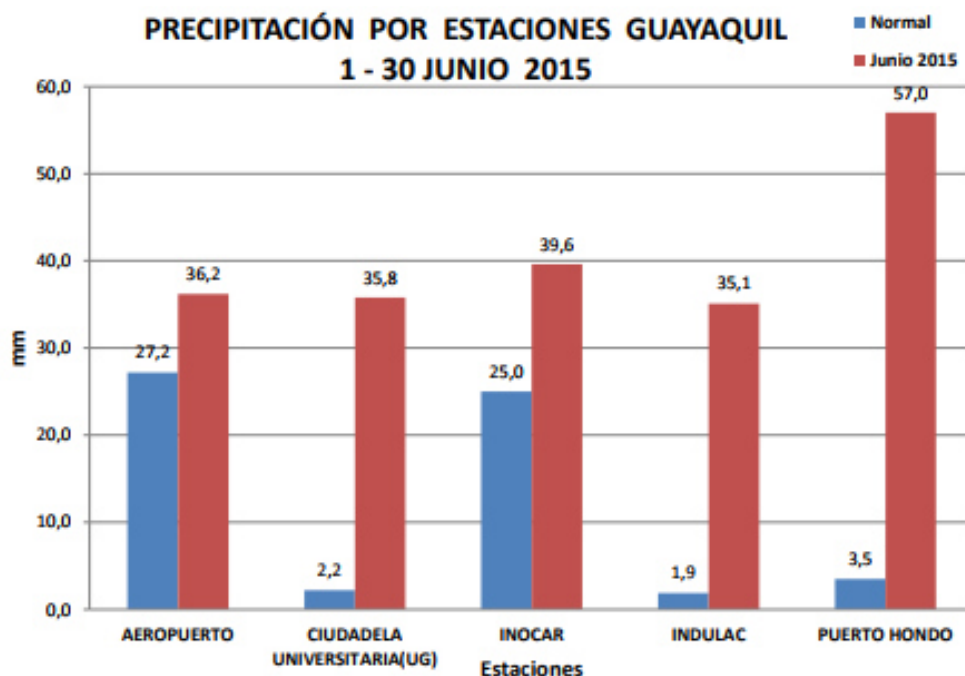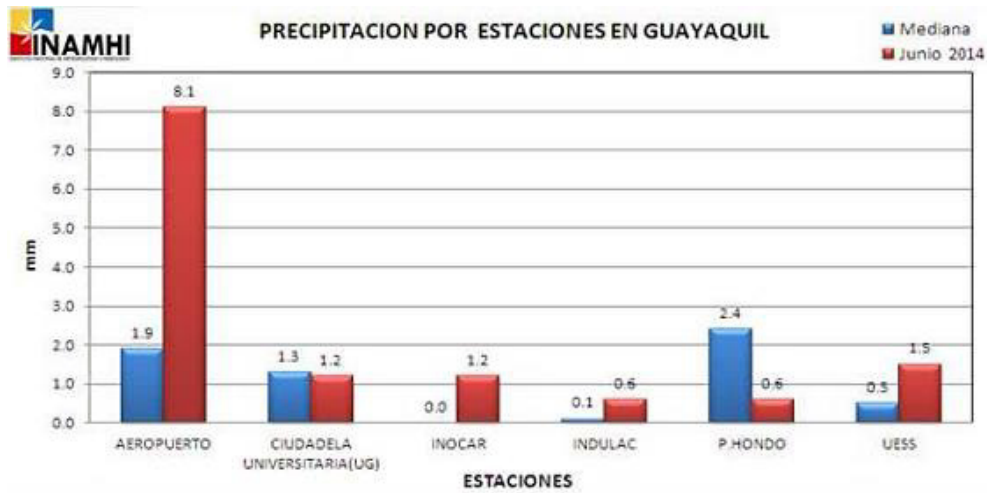
Figure 1.9.- Precipitation by stations in Guayaquil during the month of June 2014. Source: INAMHI [18].

- June 5, 2014

  No precipitation was recorded in the city, except for the INOCAR station with 1 mm [28].

- June 12, 2014

  No precipitation was recorded in the city [29].

Figure 1.10.- Daily precipitations in Guayaquil during April and June of 2014 and 2015. Source: INAMHI [18], [19], [21], [22], [24], [25], [27], [28].

Mean precipitation (Data source: INAMHI)
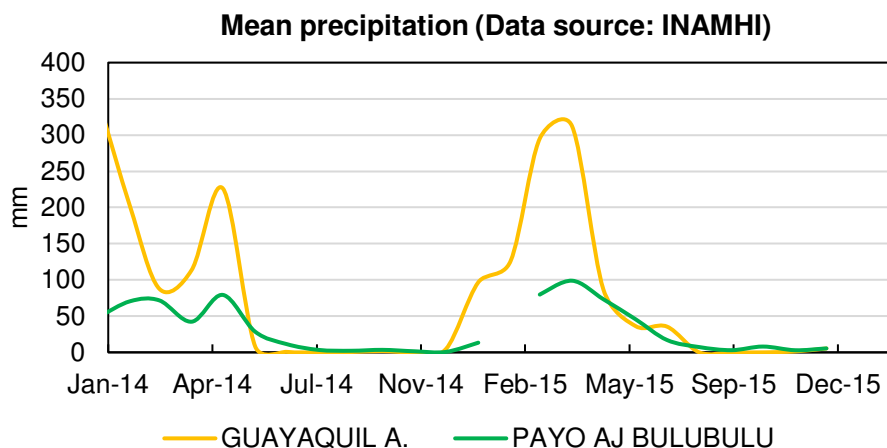
Figure 1.11.- Mean precipitation in Guayaquil A. and Payo Aj Bulubulu meteorological stations. Source: INAMHI

1.6. Flow discharges

Figure 1.12 shows that the flows at the Daule en la Capilla hydrological station in 2014 remained below 300 m³/s except for the first four months of the year corresponding to the wet season, in which the flows exceeded this value reaching a maximum of 554 m³/s in February. In 2015, the flows were above 300 m³/s from February to July, during this period a maximum of 771 m³/s was recorded in the month of April. Between August and November, during the dry season, the lowest flows of the year were recorded.

Water discharges (Data source: INAMHI)
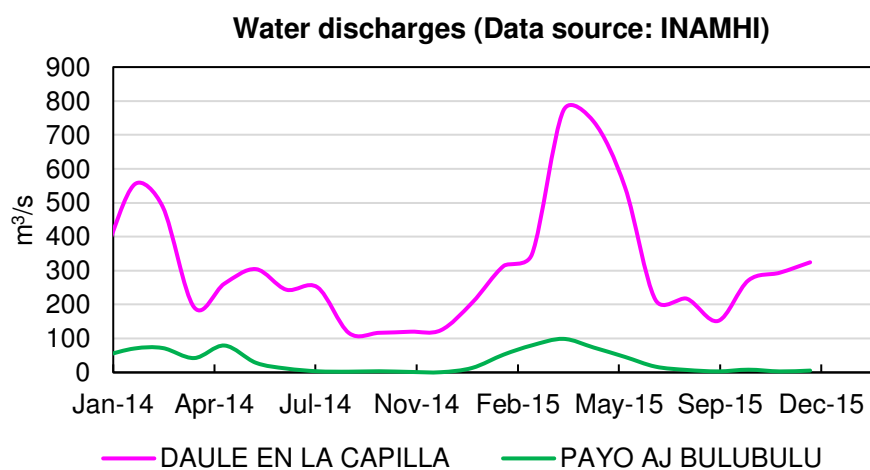
Figure 1.12.- Mean flow discharges from Daule en la Capilla and Payo Aj Bulubulu hydrological stations. Source: INAMHI

1.7. Delft3D Model

1.7.1. Overview of Delft3D and the FLOW module

The Delft3D model is a three-dimensional numerical modelling suite developed by the Deltares research institute in the Netherlands. This computational tool can be applied in 2D or 3D mode to model flows, waves, sediment transport, water quality, morphodynamical and ecological processes of coastal areas, rivers, inlets, estuaries or lakes by changing the number of layers. The modeling system is composed of several modules for different domains of interest and processes (Figure 1.13), such as: hydrodynamics, salinity, temperature, sediment transport and morphology (FLOW/MOR); short wave propagation (WAVE); water quality (WAQ); sediment transport (SED); ecological processes (ECO), particle tracking and oil spill (PART) [30].
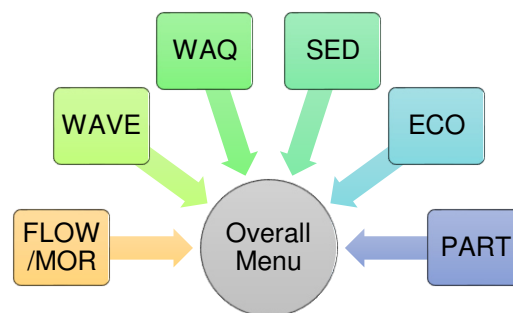
Figure 1.13.- DELFT3D modules.
Source: Author's elaboration based on Deltares in [30]

The Delft3D-FLOW module is a multi-dimensional hydrodynamic simulation program that is included in the Delft3D software package. The purpose of the module is to simulate the flow patterns in bodies of water solving the Navier-Stokes equations for an incompressible fluid and considering the Boussinesq assumptions. The simulations consider tidal, meteorological and wave forcing. Besides, the equations are calculated on a rectilinear or curvilinear staggered grid through a finite-difference code. [30].

According to Deltares in [31], the FLOW module of Delft3D works considering several assumptions for simulations in 2D or 3D and according to the simulated processes. Assumptions applicable for the simulation explained in the present work are: the curvature of the earth is not taken into account for a simulation in a Cartesian frame of reference and density is considered only in the term of pressure.

1.7.1. Staggered grid

In Delft3D-FLOW a staggered grid is applied, this means that the quantities for some of the variables of the model are defined in different positions of the numerical grid as shown in figure 1.14. Therefore, quantities for water level, salinity, temperature and

concentration of substances are computed at grid cell centers, meanwhile horizontal velocity components are defined at the midpoints of the grid cell faces [31].

The application of staggered grids offers several advantages since it facilitates the application of border conditions in a simpler way. Additionally, it is possible to use less discrete state variables obtaining the same precision as in other non-staggered grids. On the other hand, this type of grid for shallow waters prevents the generation of spatial oscillations
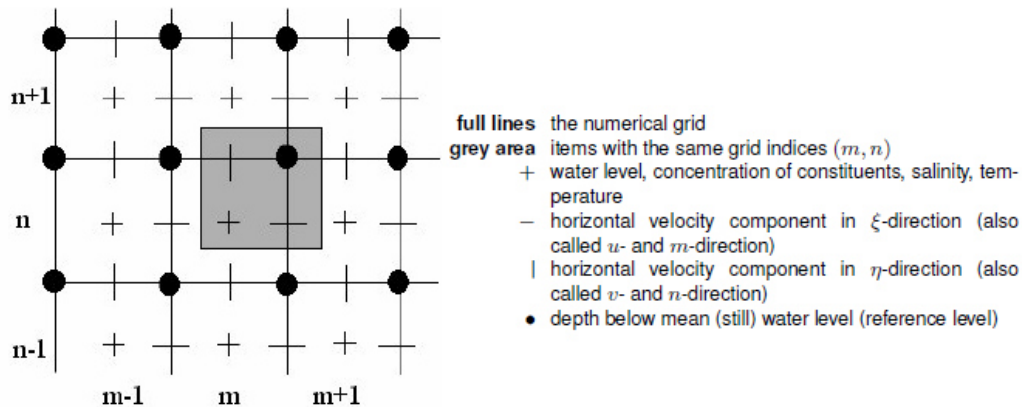
Figure 1.14.- Staggered grid. Source: Deltares [30]

1.7.2. Hydrodynamic equations

The model can be built using orthogonal curvilinear coordinates in the horizontal direction supporting orthogonal Cartesian (ξ, η) or spherical (λ, ϕ) coordinate systems. The following hydrodynamic equations in this section have been obtained and described according to what is explained in the Delft3D-FLOW user manual by Deltares in [31]. To understand in more detail the following equations of the model, consider the figure 1.15.
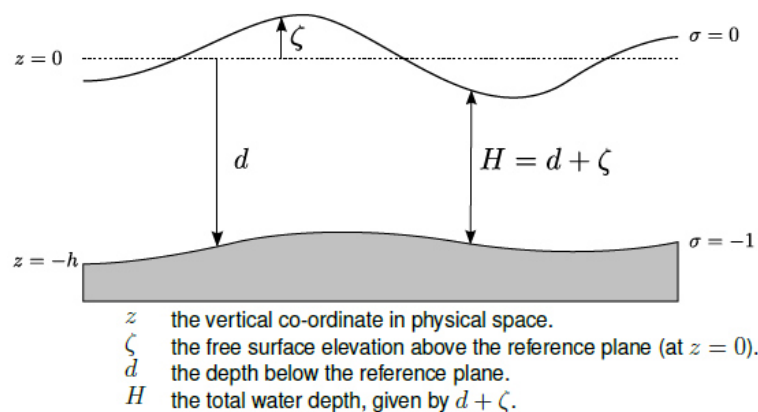
Figure 1.15.- Water level (ζ), depth (h) and total depth (H) definition in the DELFT3D model. Source: Deltares [30]

Continuity equation

Through the integration of the continuity equation for incompressible fluids over the total depth, the continuity equation for depth-averaged is obtained (Equation 1.1). The coefficients used to transform curvilinear coordinates to rectangular coordinates are represented by $\sqrt{G_{\xi\xi}}$ and $\sqrt{G_{\eta\eta}}$. The kinematic boundary at the water surface as well as at bed level are also included.

$$\frac{\partial \zeta}{\partial t} + \frac{1}{\sqrt{G_{\xi\xi}}\sqrt{G_{\eta\eta}}}\frac{\partial((d+\zeta)U\sqrt{G_{\eta\eta}})}{\partial \xi} + \frac{1}{\sqrt{G_{\xi\xi}}\sqrt{G_{\eta\eta}}}\frac{\partial((d+\zeta)V\sqrt{G_{\xi\xi}})}{\partial \eta} = (d+\zeta)Q \quad (1.1)$$

In equation 1.1, U and V represent the depth averaged velocities and Q the contribution per unit area due to the discharge or withdrawal of water, evaporation and precipitation. (Equations 1.2 and 1.3). In Q (Equation 1.4), q_{in} and q_{out} represent local sources and water sinks per unit volume; *P* is the non-local source of precipitation and *E* the non-local evaporation sink.

$$U = \frac{1}{d+\zeta}\int_{d}^{\zeta} u \, dz = \int_{-1}^{0} u \, d\sigma \quad (1.2)$$

$$V = \frac{1}{d+\zeta}\int_{d}^{\zeta} v \, dz = \int_{-1}^{0} v \, d\sigma \quad (1.3)$$

$$Q = \int_{-1}^{0}(q_{in}-q_{out})d\sigma + P - E \quad (1.4)$$

Momentum equations in the horizontal direction

The momentum equations in the ξ and η and direction are given by equations 1.5 and 1.6:

$$\frac{\partial u}{\partial t} + \frac{u}{\sqrt{G_{\xi\xi}}}\frac{\partial u}{\partial \xi} + \frac{v}{\sqrt{G_{\eta\eta}}}\frac{\partial u}{\partial \eta} + \frac{w}{d+\zeta}\frac{\partial u}{\partial \sigma} - \frac{v^2}{\sqrt{G_{\xi\xi}}\sqrt{G_{\eta\eta}}}\frac{\partial \sqrt{G_{\eta\eta}}}{\partial \xi} + \frac{uv}{\sqrt{G_{\xi\xi}}\sqrt{G_{\eta\eta}}}\frac{\partial \sqrt{G_{\xi\xi}}}{\partial \eta} - fv =$$

$$-\frac{1}{\rho_0\sqrt{G_{\xi\xi}}} P_\xi + F_\xi + \frac{1}{(d+\zeta)^2}\frac{\partial}{\partial \sigma}\left(vv\frac{\partial u}{\partial \sigma}\right) + M_\xi \quad (1.5)$$

$$\frac{\partial v}{\partial t} + \frac{u}{\sqrt{G_{\xi\xi}}}\frac{\partial v}{\partial \xi} + \frac{v}{\sqrt{G_{\eta\eta}}}\frac{\partial v}{\partial \eta} + \frac{w}{d+\zeta}\frac{\partial v}{\partial \sigma} + \frac{uv}{\sqrt{G_{\xi\xi}}\sqrt{G_{\eta\eta}}}\frac{\partial \sqrt{G_{\eta\eta}}}{\partial \xi} - \frac{u^2}{\sqrt{G_{\xi\xi}}\sqrt{G_{\eta\eta}}}\frac{\partial \sqrt{G_{\xi\xi}}}{\partial \eta} + fu =$$

$$-\frac{1}{\rho_0\sqrt{G_{\eta\eta}}} P_\eta + F_\eta + \frac{1}{(d+\zeta)^2}\frac{\partial}{\partial \sigma}\left(vv\frac{\partial v}{\partial \sigma}\right) + M_\eta \quad (1.6)$$

In the above equations the density variations are negligible except in terms of baroclinic pressure, Pξ and Pη represent the terms of pressure gradients. The vertical eddy

viscosity coefficient is represented by vv. On the other hand, Fξ and Fη, represent the forces of unbalanced horizontal Reynold's stresses. The contributions from sources or sinks of momentum are represented by the Mξ and Mη terms.

Coriolis force

The Coriolis force is influenced by the geographic latitude and the angular speed of rotation of the earth. The equation 1.7 describes the Coriolis parameter f, which must be specified according to the specific area to be modeled.

$$f = 2\Omega \sin \phi$$

(1.7)

1.7.3. Spatial and temporal resolution

The spatial resolution of the model is built working with the RFGRID module of Delft3D. In this module the grid is created according to the domain of the model and its optimal resolution is defined, which is obtained by complying with certain grid quality criteria (orthogonality, aspect ratio and smoothness). In this way, it avoids generating mathematical instabilities and the collapse of the model.

The Courant Number is the main parameter to be considered to achieve numerical stability. Its value is verified in the QUICKIN module of Delft3D and should not be greater than 10, however, it can be greater if there are problems with very small spatial and temporal variations. In the equation 1.8, Δt represents the time step in seconds, g the gravitational acceleration, H the total water depth and $\{\Delta x, \Delta y\}$ represents the grid spacing in the *x* and *y* direction according to Deltares.

$$C = \frac{\Delta t \sqrt{gH}}{\{\Delta x, \Delta y\}}$$

(1.8)

The time-step is an always positive value that is defined considering the courant number, both parameters are closely related to each other. On the other hand, it is important to consider that the start and end time of the simulation must be integer multiples of the time-step. Therefore, to ensure that the model works according to an adequate temporal and spatial resolution, it is advisable to do several tests by changing the Courant Number and evaluate its effect on the results.

CHAPTER 2

2. METHODOLOGY

In the diagram below (Figure 2.1) the general methodology applied throughout the project is summarized, which ranges from the definition of the problem to be solved to the analysis of results. In this study, as described in this chapter, the modeled results were obtained at a time scale of 10 min and the spatial resolution was found in a range of 500 m - 1km in the internal zone of the Gulf and 4 km in the external zone.
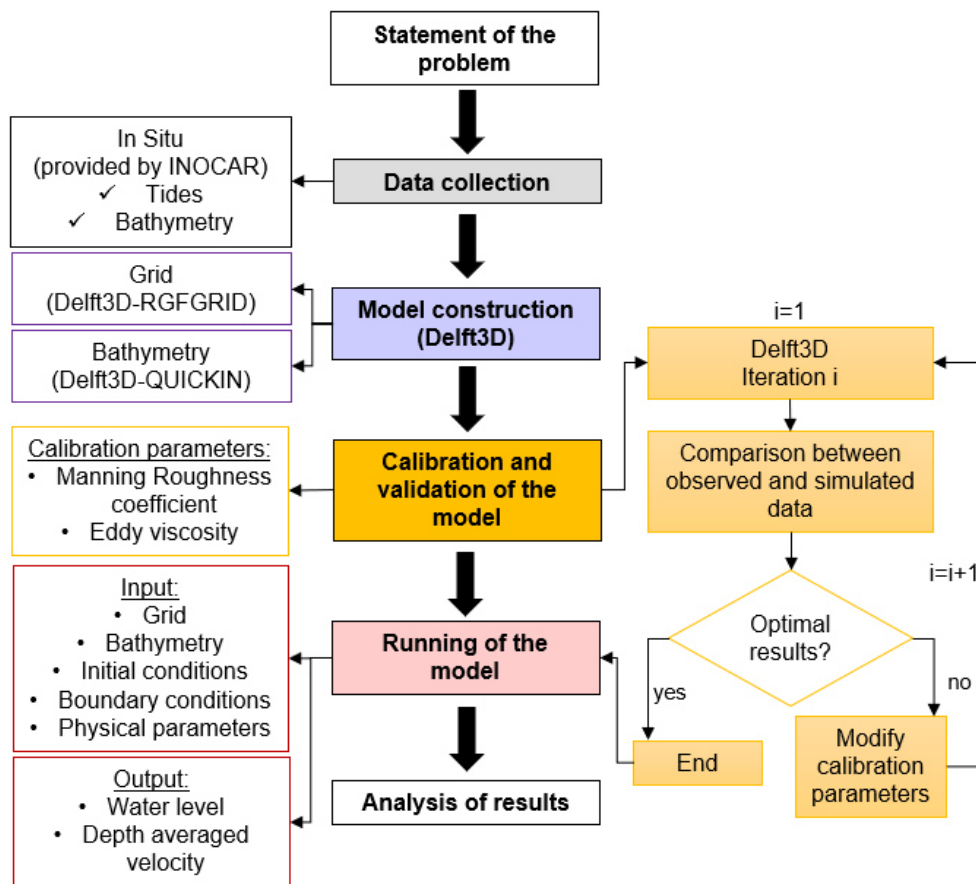
Figure 2.1.- Diagram of the methodological process. Source: Author's elaboration

2.1. MODEL SET-UP

2.1.1. Available data (Input data)

Bathymetry

The bathymetric dataset of the study area was provided by the Ecuadorian National Oceanographic Institute of Navy (INOCAR). The resolution of the bathymetry in the outer part of the Gulf was coarser in contrast to the resolution in the inner part. Besides, depths in the internal channels reach up to approximately 20 m increasing towards the outlet of

the gulf where in the outermost zone the depths vary between 800 and 1000 m. It is important to consider, that the bathymetry provided did not cover the whole inner estuary but just the area to be modeled, as seen in figure 2.5.

Tides

The data of tide level used for the model set-up and calibration was provided by INOCAR and consisted in hourly time-series measurements for the months of April and June of 2015-2016 from the tide gauges of Anconcito, Data Posorja, Puna and Puerto Bolivar.

2.1.2. Grid and domain extent

The grid covers the Gulf of Guayaquil extending from the Sprig of Santa Elena to approximately 34 km towards the interior of the estuary taking the Cascajal channel as a reference. The total study domain is composed of 55 cells in the M-direction and 121 cells in the N-direction, covering an approximate area of 155x172 km considering the wider sections of the mesh. The grid spatial resolution ranges from 500 m - 1 km in the inner Gulf area to less than 4km in the outer zone.

Numerical grid generation process

A curvilinear grid in Cartesian coordinates was built using the RGFGRID program of Delft3D. The curvilinear characteristic of the grid allows the dimensions and shape of cells which are initially rectangular to be slightly modified to fit the shape of the study area. In spite of this, the details of the coastal morphology of very complex areas cannot be represented very accurately to reality since, there is a limit to the curvature and variation of cell size [32].

RGFGRID is a program that allows the user to build orthogonal, curvilinear grids in Cartesian or spherical co-ordinates. For the Gulf of Guayaquil grid, a cartesian co-ordinate system was selected. In addition, for the construction of the grid it is first necessary to have a land boundary file of the area for which the simulation will be carried out. This file with mask (*.ldb) contains the coordinates of each polyline representing the coastline and helps to define the grid for the model area as explained in [33] .

The grid construction was made in RGFGRID by generating longitudinal and transverse splines over the study area represented by the land boundary file, which were then transformed into the grid as the figure 2.2 and 2.3 shows. For the grid to meet the quality criteria (orthogonality, aspect ratio and smoothness) this process is carried out several times, so that the grid with the best conditions for the simulation is obtained.
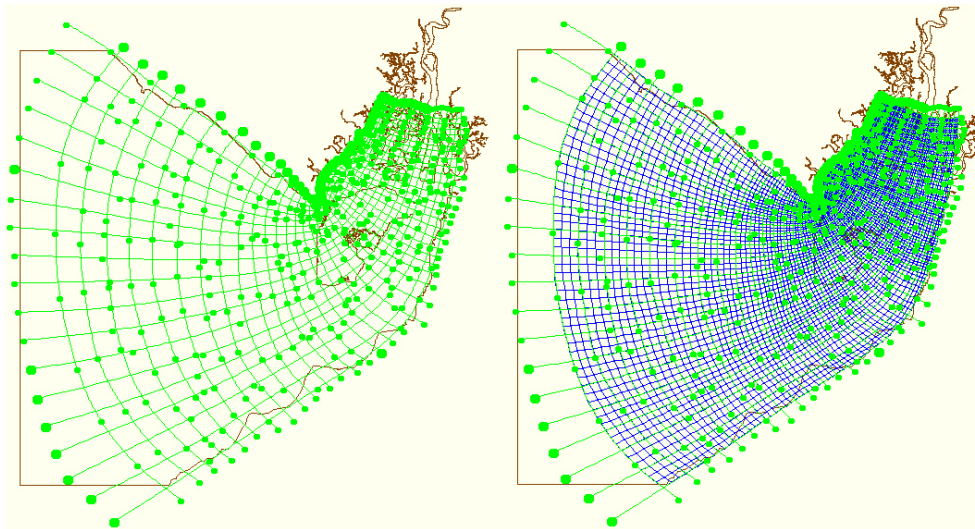
Figure 2.2.- Splines (left) and grid created from splines (right) created in RFGRID.

Source: Author's elaboration
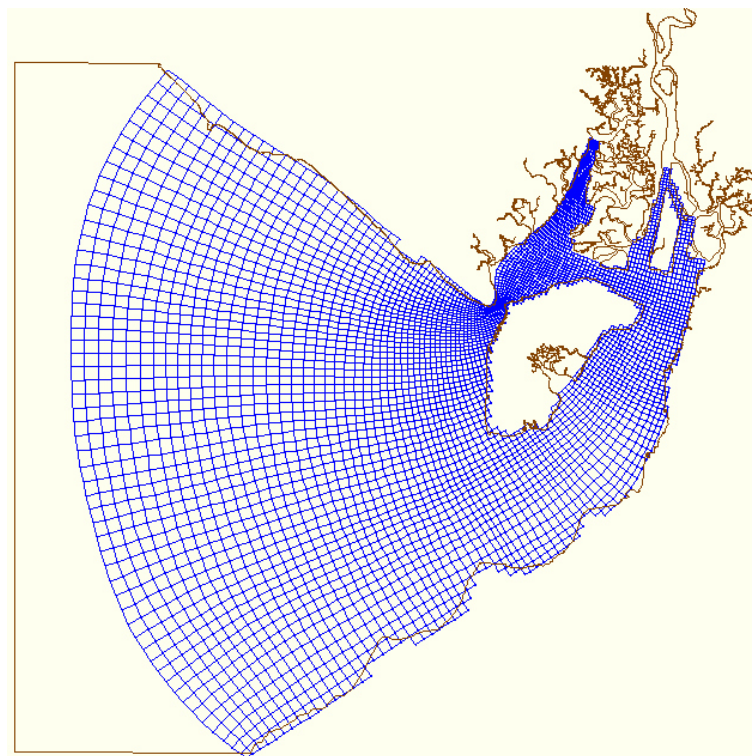
Figure 2.3.- Final grid built in RFGRID. Source: Author's elaboration

The three grid quality conditions were evaluated in RFGRID. If the grid does not fulfill the orthogonality condition, RGFGRID allows the user to orthogonalise the grid to improve this quality parameter. The refined final grid for the Gulf of Guayaquil fulfilled the orthogonality, aspect ratio and smoothness conditions. Therefore, it was saved in a file with mask (*.grd) along with a grid enclosure file with mask (*.enc) that will be used on Delft3D-FLOW. The domain grid extent is shown in figure 2.4.

P1: (-80.99, -2.20)
P2: (-80.24, -2.73)
P3: (-80.01, -2.35)
P4: (-79.84, -2.42)
P5: (-80.80, -3.77)
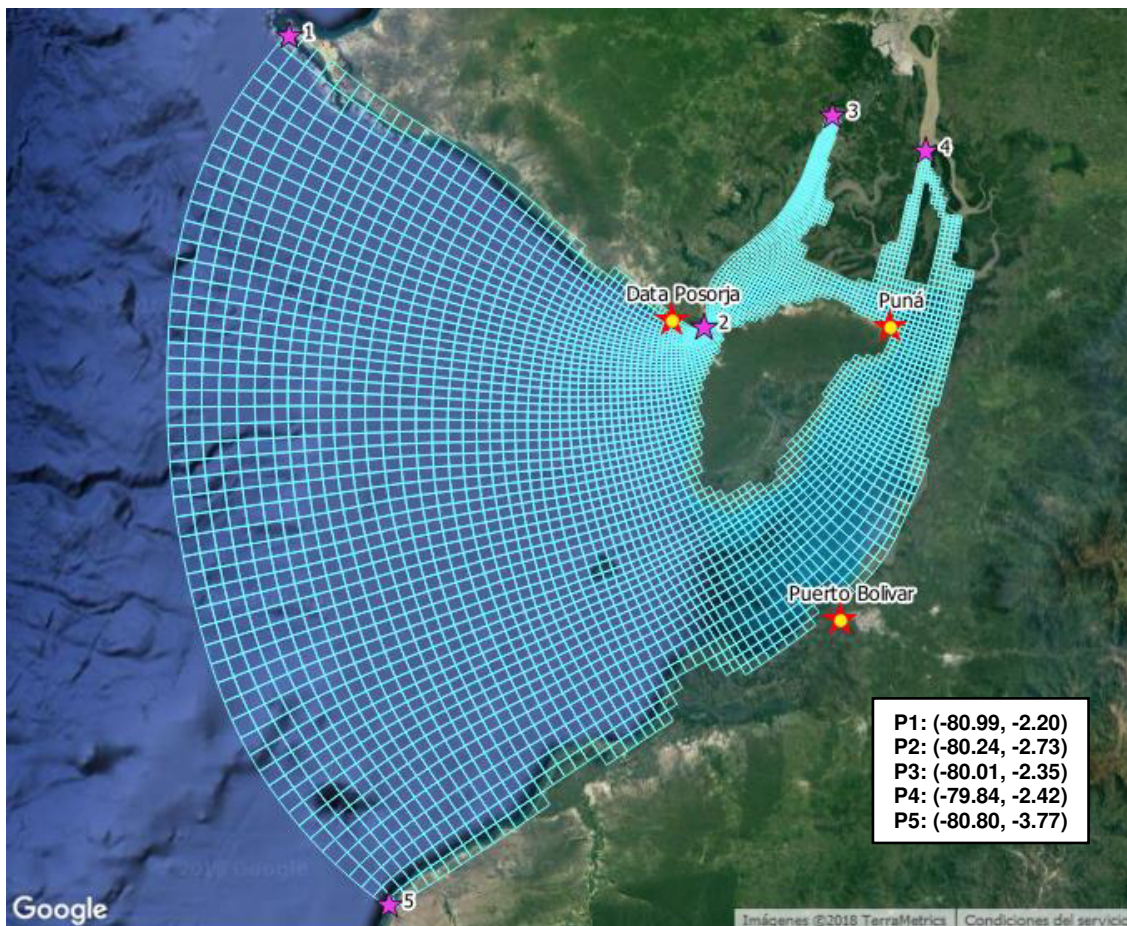
Figure 2.4.- Domain grid extent and tide gauges from INOCAR in the Gulf of Guayaquil. The study area covered by the grid is between P1, P2, P3, P4, P5 points. Source: Author's elaboration.

2.1.3. Bathymetry

To perform the simulation in Delft3D-FLOW it is necessary to use a file with mask (. *dep) that contains the bathymetry of the study area, which can be uniform or spatially variable. This file is created in the QUICKIN tool of Delft3D, which as explained in [34], is a program for the generation, interpolation, manipulation and visualization of variables that vary spatially such as bathymetry. The operations menu in QUICKIN has most of the options that are used during the (. *dep) file generation process.

In order to create the (. *dep) file, the bathymetry data must be saved in a sequential list with format *x, y, z* within a file with mask (. *xyz), then loaded in the QUICKIN program along with the grid. It is important to considerer that in Delft3D the depth values are positive downwards, then if the data obtained has the opposite format, QUICKIN allows the user to multiply the values for the model area by -1.

Two interpolation methods are available in QUICKIN, grid cell averaging and triangular interpolation. Both methods can be used in the same model area by defining polygons

for each area and selecting the desired interpolation method. For the Gulf area with a bathymetry of higher resolution than the grid the grid cell averaging interpolation method was used, while for the external area of the Gulf with less depth points than grid points the triangular interpolation method was applied.

Not all the grid points had depth values as seen in figure 2.5 (left), therefore, after the interpolation the cells with missing values were filled with an internal diffusion mechanism. Finally, because the bathymetry provided was referred to the MLWS (Mean Low Water Spring), a uniform value that represented the difference in depth from the MLWS to the MWL (Mean Water Level) was added to the depth. This values were obtained from the Table of Tides of INOCAR in [35]. The final bathymetry is shown in figure 2.6.
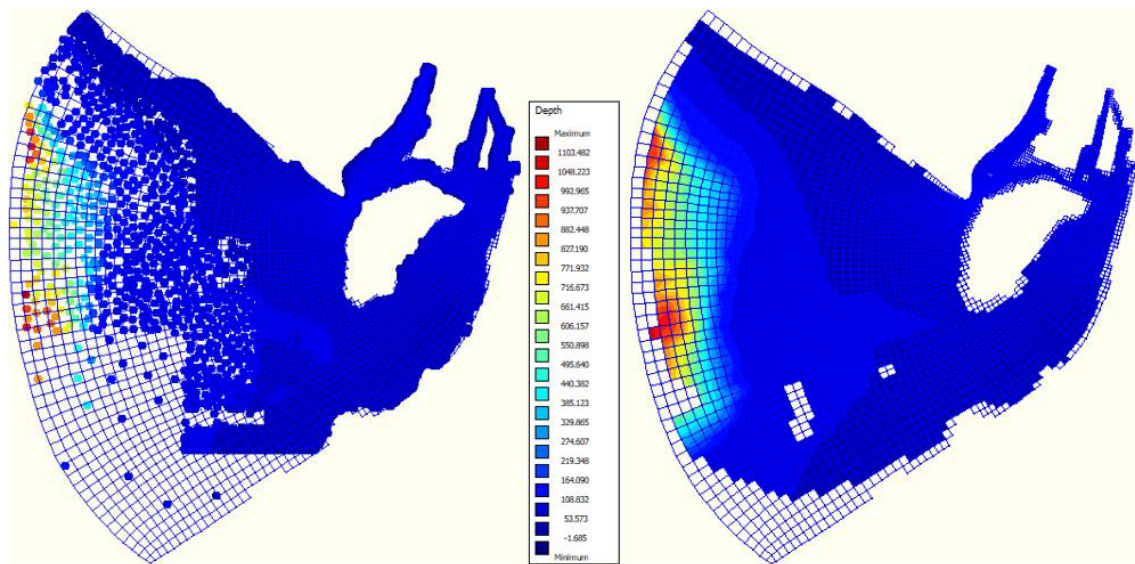
Figure 2.5.- Bathymetry interpolation in QUICKIN. Bathymetry samples (left) and interpolated bathymetry (right). Source: Author's elaboration.
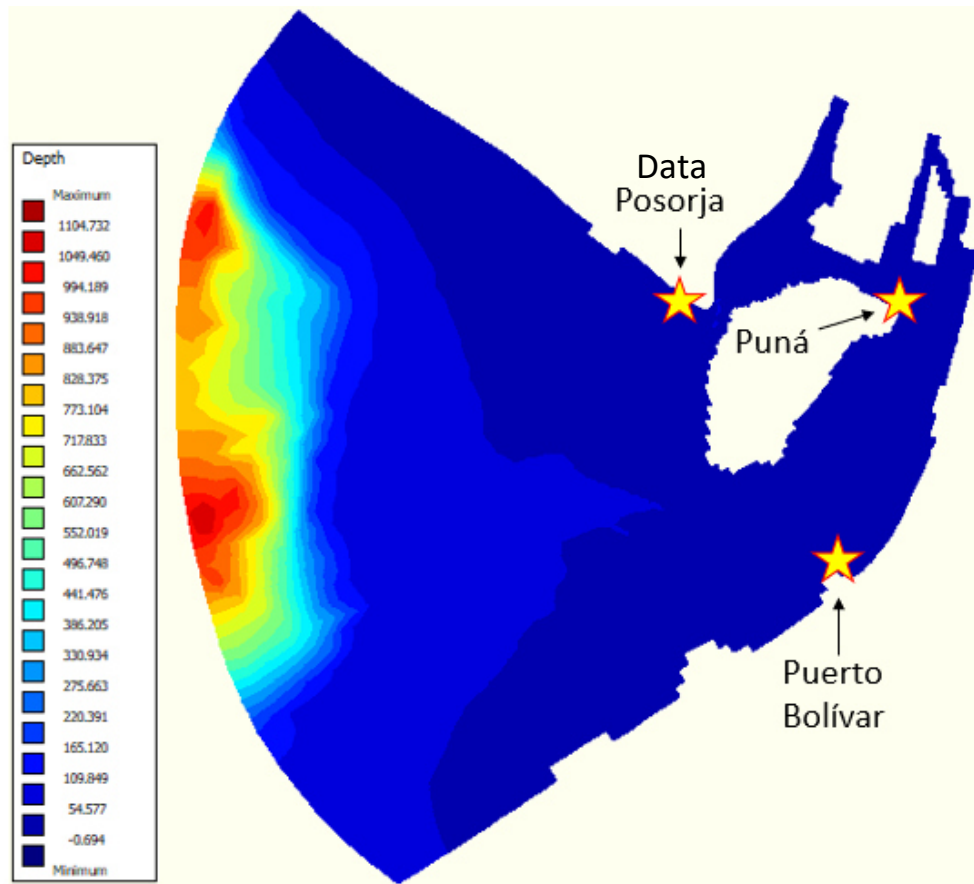
Figure 2.6.- Final bathymetry of the Gulf of Guayaquil and Data Posorja, Puna and Puerto Bolivar tide gauges locations. Source: Author's elaboration.

2.1.4. Boundary conditions

The open boundaries conditions represent the influence of the outer world and they should be defined far away from the areas of interest [31]. The Gulf of Guayaquil model includes one open boundary located at mouth of the outer estuary. Water level conditions were used while the hydrodynamic forcing was prescribed using astronomical and time-series components for each simulation case.

For this study the Anconcito tide gauge data located at the northern end of the boundary section was used as open boundary conditions. Because of the lack of data at the southern end of the boundary it was assumed that water levels at both ends of the open boundary were the same. According to Deltares in [31], the values between these two points are linearly interpolated.

The hourly time-series water level data provided by INOCAR was interpolated using a spline interpolation to create a 10-min time-series dataset. This was done because the results of the simulation using the tidal hour data showed a good fit with the observed data, however, in the highs and lows an instability was generated that produced irregular peaks in the wave. The difference between the curve corresponding to the hourly tides

and the tides interpolated every 10 min is shown in the figures 2.7 and 2.8. Additionally, the reflection parameter alpha whose higher values makes the open offshore water level boundary less reflective for short wave disturbances that propagate towards the boundary at the start of the computation [36] [31], was set to a typical value of 100.
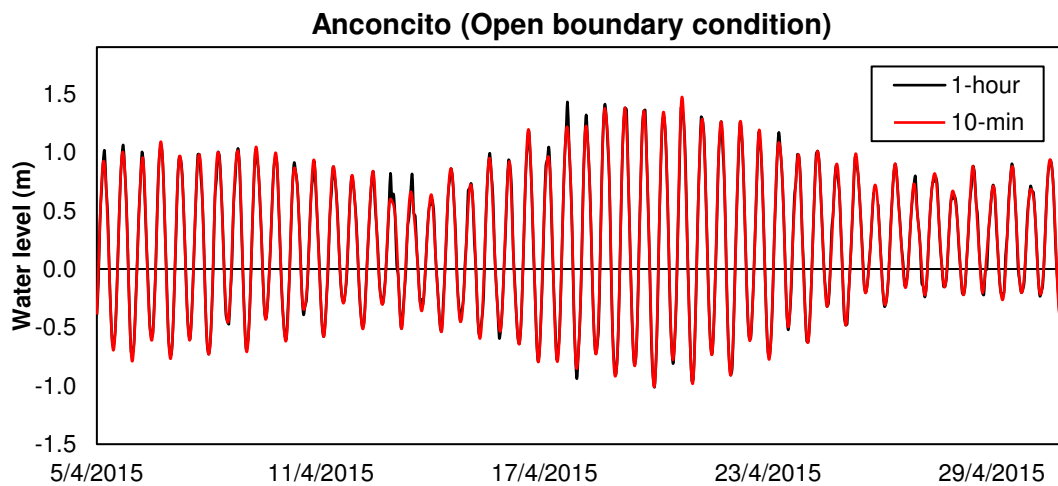
Figure 2.7.- Anconcito time-series data used as boundary condition. The black line represents the original provides data by INOCAR at an interval of 1 hour, the red line represents the interpolated data to an interval of 10 min. Source: Author's elaboration.
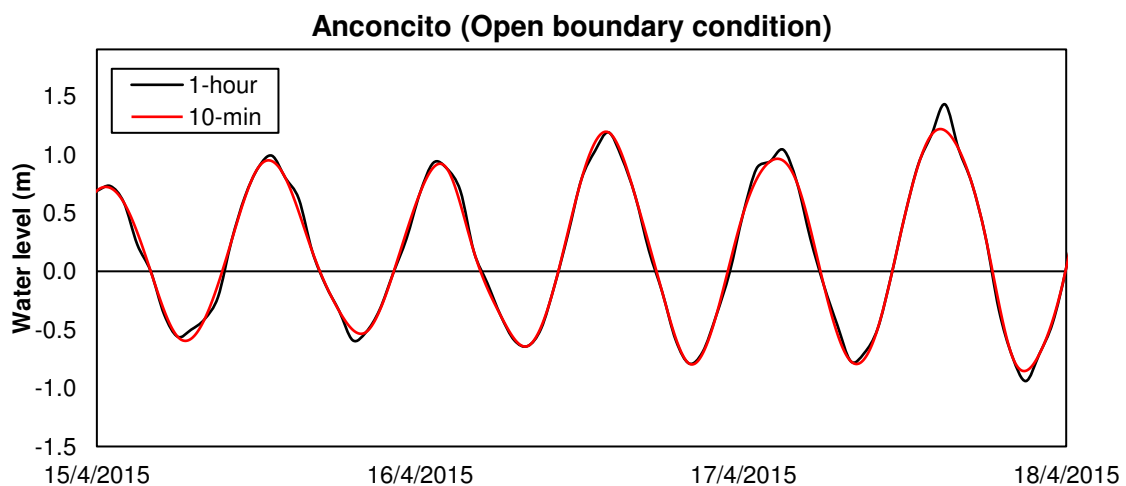
Figure 2.8.- Anconcito time-series data at an interval of 1 hour (black line) and interpolated data to an interval of 10 min (red line). Source: Author's elaboration.

CHAPTER 3

3. CALIBRATION AND VALIDATION

3.1.1. Calibration

The model was calibrated for water level by changing two physical parameters, the Manning friction coefficient and the Eddy viscosity. The optimal values of these parameters were determined from the comparison between the simulated data with the observed data in the tidal stations of Data Posorja, Puna and Anconcito. For this purpose, several simulations were carried out, calculating the statistical indicators for each monitoring station and then a global result.

The time period used for the calibration process was the month of April 2015, since it had the largest amount of data available in the three tidal stations selected for comparison. In the case of the months of April and June 2014 there were only data available from the Puna station, while for the month of June 2015 although there were data from the three stations, they had several missing data that decreased the amount of information available. However, statistical indicators were calculated for June 2015 using the calibrated parameter values of April 2015.

To calibrate the model according to the coefficient of friction of Manning, values between 0.012 $s/m^{1/3}$ and 0.030 $s/m^{1/3}$ were considered. Taking as reference this range of values for the calibration of water level from the study of Barrera in the Guayas river estuary of Ecuador [37]. The eddy viscosity was calibrated by tuning its value between a range of 10 m^2/s to 100 m^2/s. According to Deltares in 2016, for large tidal areas with a grid size of more than hundreds of meters, as in this study, the typical eddy viscosity values are within that range [31].

Statistical indicators

- **Skill index**

The skill index has been used in previous studies, see [38], [39], for the calibration of models. This indicator allows to quantify the goodness of fit of the model, which is a measure of the normalized error of its predictive capability. Values of skill score close to 1 are expected, since a skill score of 0 indicates model mismatch [38], [40].

- **Correlation coefficient**

This parameter ranges from 0 to 1 and it indicates how well the observed data is replicated by the model or how similar the behavior of both water level data sets is. The

higher its value is, the better the correlation between both data sets is. This is a statistical indicator commonly used for the calibration of models, see [37] , [38], [39], [41],

- **Root-mean-square error (RMSE)**

RMSE represents the absolute deviation between predicted and observed values and it is a statistical parameter used frequently by different authors during the model calibration process as found in [37], [38], [39], [41], [42]. The greater the value of the RMSE, the greater the error or difference between the two data sets. Therefore, the expected values of RMSE should be close to 0.

Tidal stations	RMSE	R^2	Skill
Data Posorja	0,181	0,929	0,980
Puna	1,206	0,373	0,499
Puerto Bolivar	0,177	0,956	0,988
Global mean	**0,521**	**0,752**	**0,822**

Table 1.- Best statistical indicators values obtained from the calibration process.

The best simulation was obtained with a Manning friction coefficient of 0.030 s/m$^{1/3}$ and Eddy viscosity of 50 m^2/s. Of the three stations, Puerto Bolivar and Data Posorja present the most optimal values of the statistical indicators (Table 1). The values for Skill index and R^2 are very close to 1, whereas the values of RMSE are close to 0 as expected. Although statistical indicators from the Puna station are not the most satisfactory, they are not considered to be outside the acceptable, as it was for other simulations during the calibration. In figure 3.1 the plots between the observed and simulated data for each tidal station in April 2015 show the similarity between both datasets.

Consequently, for the simulations of June 2015 and April and June 2014 the values of Manning friction coefficient of 0.030 s/m$^{1/3}$ and Eddy viscosity of 50 m^2/s were used. Although the amount of data for the month of June 2015 to perform the calibration was not sufficient, the statistics for each station were calculated and the observed data was compared graphically with the data simulated in those stations as shown in figure 3.2. As in April 2015, in June 2015 the statistical indicators showed optimal values for the Data Posorja and Puerto Bolivar stations, and low values for the Puna station.

April 2015 - Observed versus Simulated Water Level
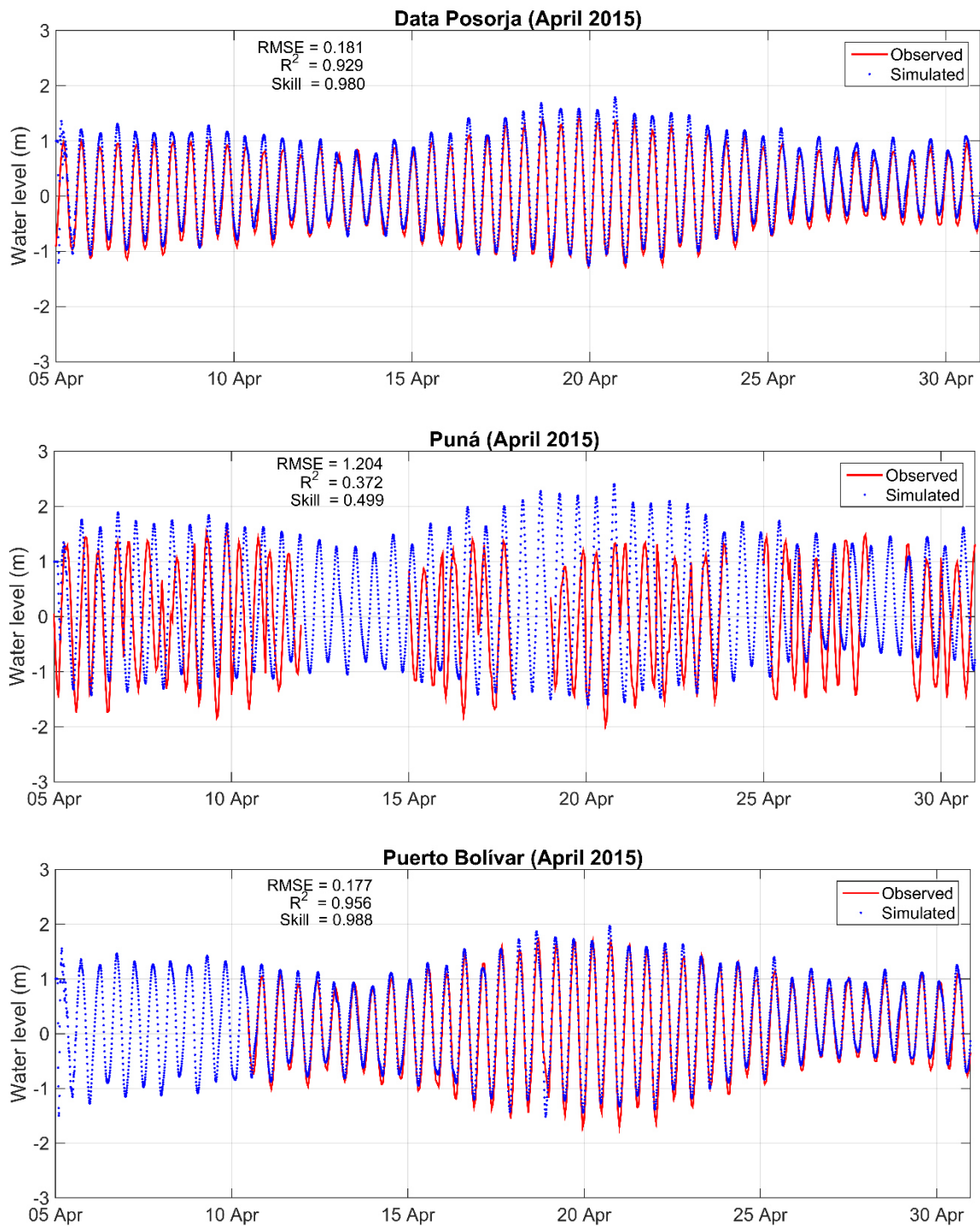
Figure 3.1.- Observed data versus simulated data of April 2015 from the tide gauges: Data Posorja, Puna and Libertador Bolivar. Source: Author's elaboration.

June 2015 - Observed versus Simulated Water Level
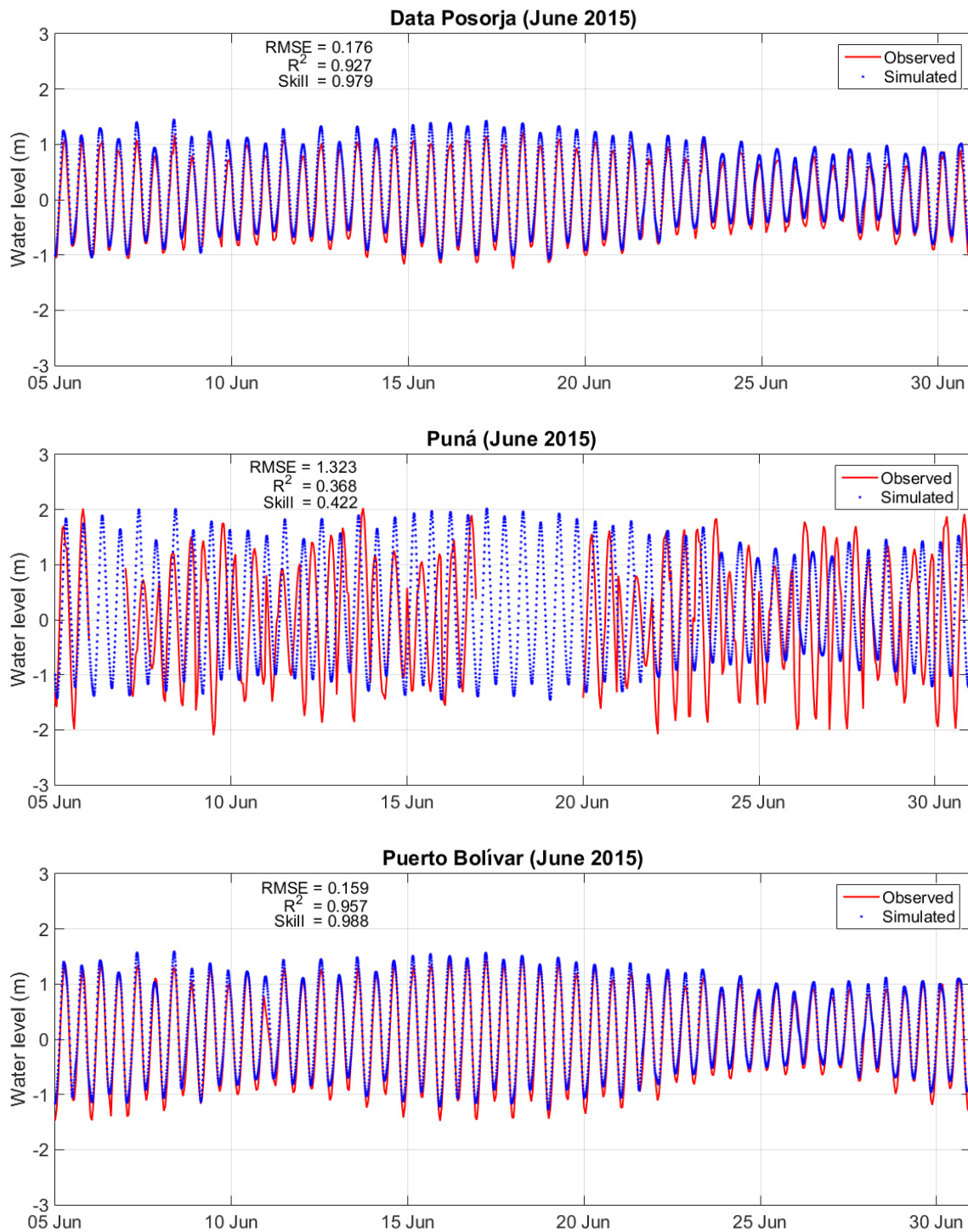
Figure 3.2.- Observed data versus simulated data of June 2015 from the tide gauges: Data Posorja, Puna And Libertador Bolivar. Source: Author's elaboration.

3.1.2. Sensitivity analysis

The sensitivity analysis showed that the model applied in this case to simulate the water level is more sensitive to changes in the Manning coefficient than to the Eddy viscosity variations, as seen in the graph 3.3 and table 2.
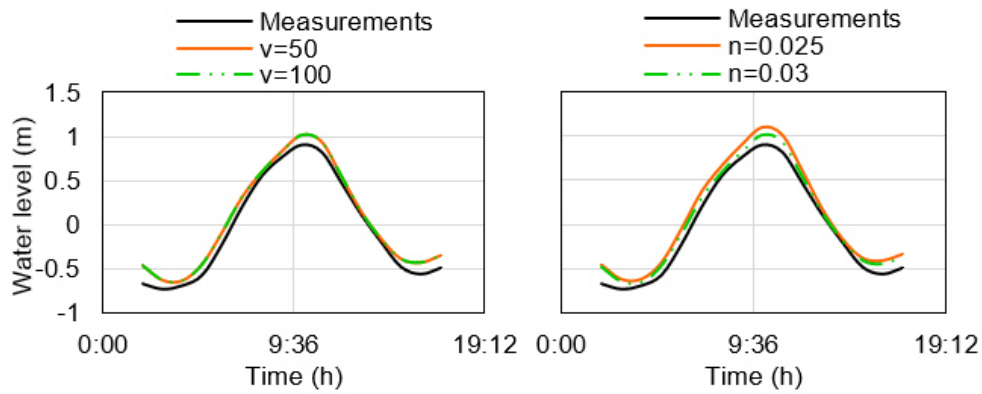
Figure 3.3.- Water level simulation results with different eddy viscosity values (50 m/s, 100 m/s) (left) and Manning coefficients (0.025, 0.03) (rigth).

Source: Author's elaboration.

Simulation	Time	Eddy Viscosity	Manning Coefficient	RMSE	R^2	Skill
1		10	0.025	0.592	0.722	0.812
2		10	0.03	0.521	0.752	0.822
3		100	0.012	3.465	0.449	0.301
4		100	0.025	0.591	0.722	0.812
5		100	0.03	0.519	0.753	0.822
6	05/04/2015-	50	0.012	3.471	0.445	0.295
7	30/04/2015	50	0.025	0.591	0.723	0.813
8		**50**	**0.03**	**0.521**	**0.752**	**0.822**
9		25	0.03	0.521	0.752	0.822
10		25	0.025	0.591	0.722	0.813
11		75	0.03	0.520	0.752	0.822
12		75	0.025	0.590	0.723	0.812

Table 2.- Summary of calibration results for water level. Source: Author's elaboration.

CHAPTER 4

4. ANALYSIS OF RESULTS

The analysis of results was performed by obtaining the tidal residual for each monitoring station from the difference of the tide data series of the El Niño 2015 year minus the 2014 normal year. Additionally, for the same years and using the water level maps obtained with the model, the tide condition and current velocity of the months of April (wet season) and June (dry season) were compared. To analyze the results during spring and neap tides, the date of each month in which this condition occurred was selected. The dates were obtained according to the Spring Tides and Lunar Phases Calendar available online on the INOCAR website in [43], see Table 3, which are indicated below:

- Spring tides (Lunar phase: New Moon)

    o April 29, 2014 vs. April 18, 2015

- Spring tides (Lunar phase: Full Moon)

    o June 12, 2014 vs. June 2, 2015

- Neap tides (Lunar phase: First Quarter)

    o April 7, 2014 vs. April 25, 2015

    o June 5, 2014 vs. June 24, 2015

		Moon phase and spring tides (Source: INOCAR)					
		New Moon	**First Quarter**	**Full Moon**	**Last Quarter**	**Perigee**	**Spring tides**
2014	**April**	29	7	15	22	22	1, 2, 16, 17, 18, 19, 29, 30
	June	27	5	12	19	14	13, 14, 15, 16, 27, 28, 29, 30
2015	**April**	18	25	4	11	16	5, 6, 7, **19, 20, 21, 22**
	June	16	24	2	9	9	3, 4, 5, 17, 18, 19
		Days highlighted with bold correspond to the highest spring tides					

Table 3.-Spring tides and lunar phases in April and June 2014/2015. Source: Author's elaboration based on INOCAR data in [42].

For the month of June 2014 there were no data available for the day 19 or from day 23, for this reason it was not possible to compare the tides during the lunar phase of the new moon or during the last quarter. Consequently, tide conditions were only compared during the dates corresponding to first quarter and full moon. All the maps of tides and velocity of currents of the Gulf presented in this chapter have been selected considering as high tide and low tide what occurred in Puerto Bolivar. Therefore, when referring to high tide and low tide this will be in Puerto Bolivar.

4.1. Tide residuals (2015 - 2014)

For each monitoring station and every month, the modeled tidal results were plotted overlapping the curves of the years 2014 and 2015 (Figures 4.1 and 4.2) matching the time of the second-high tide of the days corresponding to the moon phase full moon. The full moon dates were selected to phase the series since they allowed to maintain the largest amount of data for both years. Because, in 2015, the full moon occurred between the first days of the month and in 2014 at the middle of the month, it was not possible to include approximately 15 days in each graphic.

According to the above, it was possible to calculate the difference in tidal height between the year 2015 when there were El Niño conditions and the year 2014 considered a normal year. The figures 4.1 and 4.2 show this tidal residual for April and June of each monitoring station considered in this project: Data Posorja, Puna and Puerto Bolivar.

It was observed that, in April (Figure 4.1), the tidal residuals were greater during neap tides. In addition, of the two periods of spring tides of the month, the greatest differences in tidal height or residuals were obtained during the lunar phase of the new moon. On the contrary, during the quadrature of June (Figure 4.2) tidal residuals were lower compared to the month of April. In addition, during the syzygy phase of the new moon in April and the quadrature phase in June it was evident that during most days the tide height was higher in 2015 with El Niño conditions than in 2014 under normal conditions.

On the other hand, of the three tide stations it was in Puna for which the greatest differences in tidal height were obtained in both years. This station is located in the area of the Cascajal Channel where the tides tend to increase in part due to the reduction of the width of the channel compared to the outermost areas of the estuary. However, it is important to remember that the results of the calibration/validation stage of the model described in Chapter 3 showed that in Puna the adjustment between the observed and simulated data was approximately 50%. Consequently, the water levels obtained in the mentioned station reflect that it is very possibly that the resolution of the grid in Cascajal needs to be finer in order to obtain results more adjusted to reality.
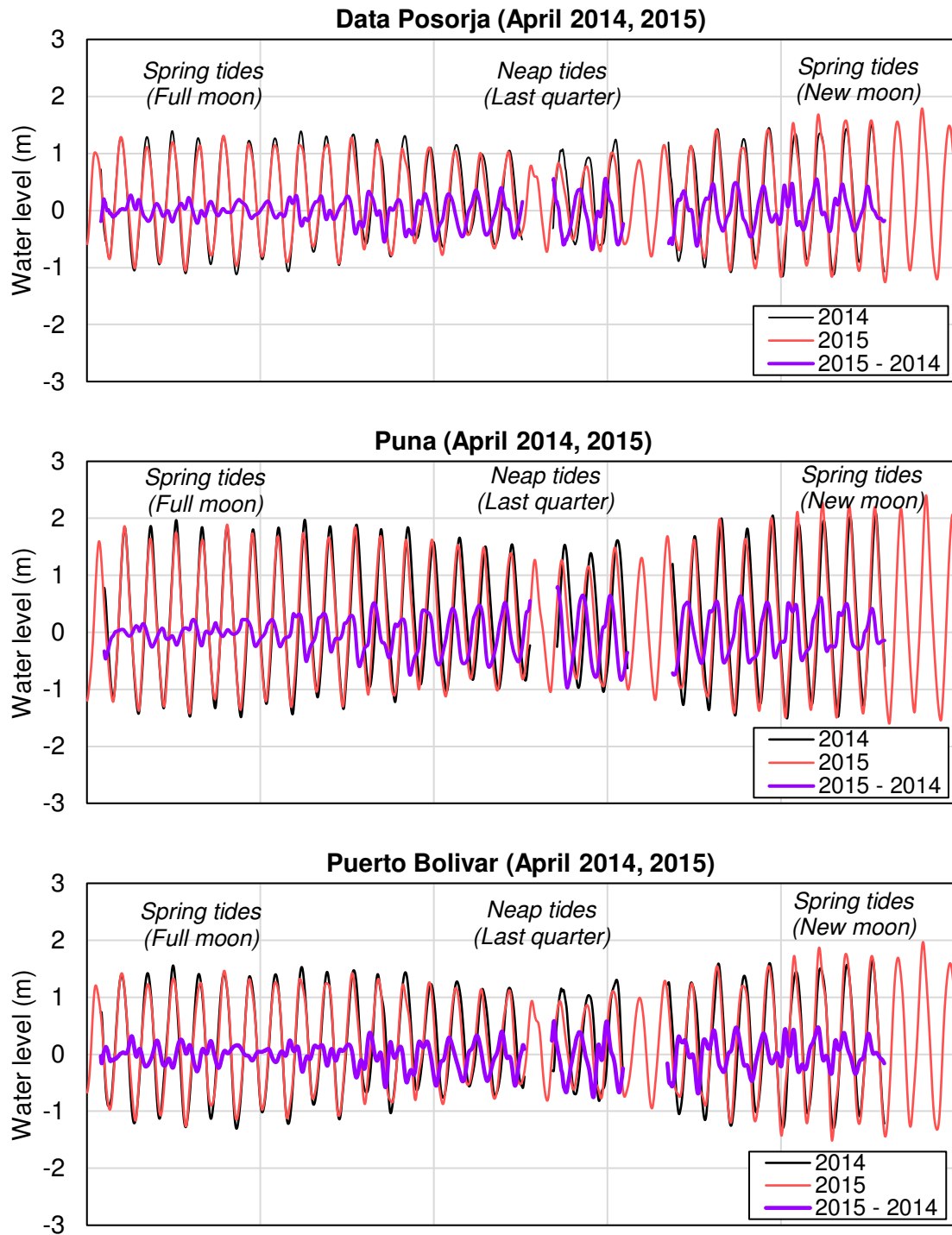
Figure 4.1.- April tide residuals (difference between 2015 and 2014) for the tide gauges of Data Posorja, Puna and Libertador Bolivar. Source: Author's elaboration.
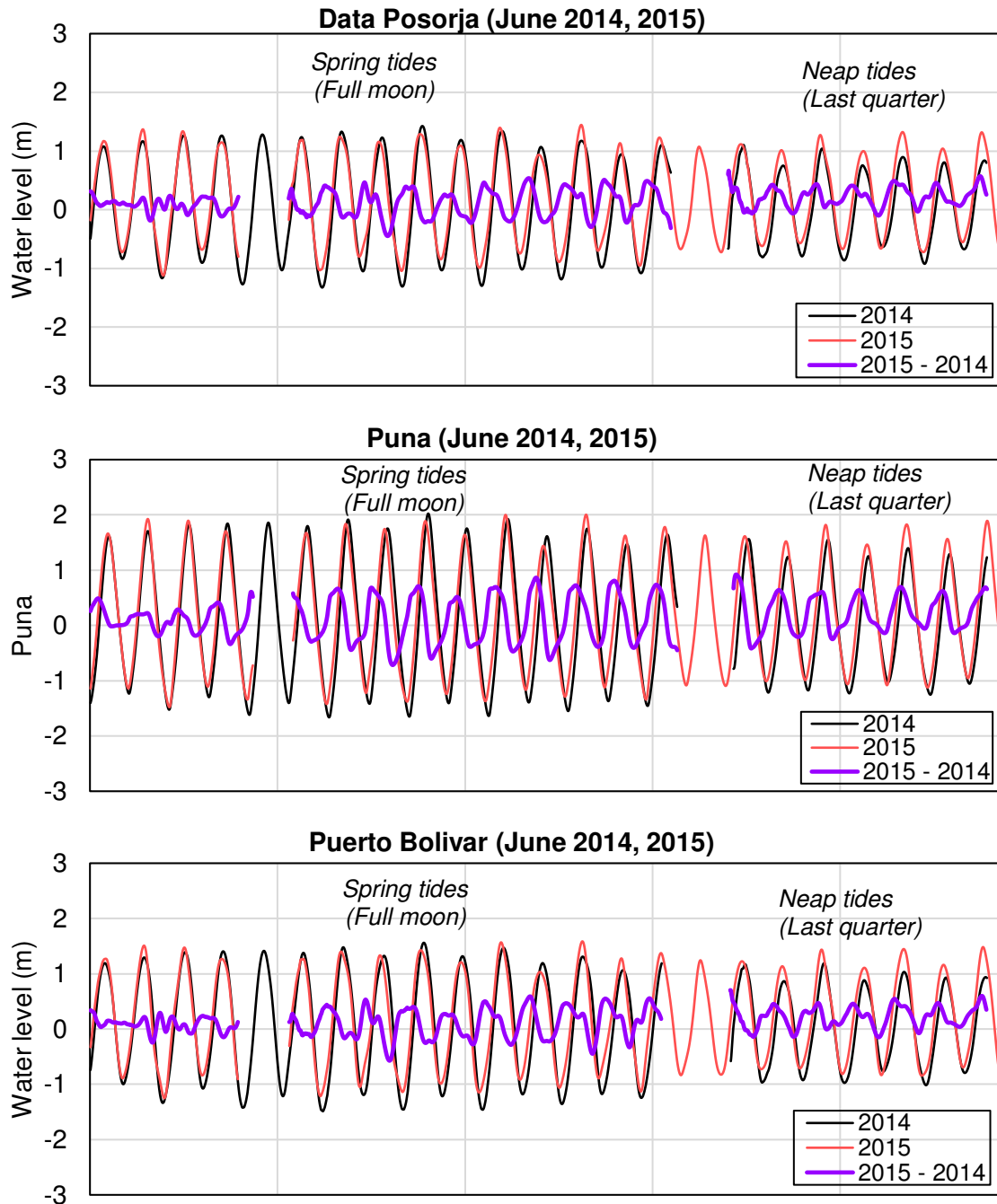
Figure 4.2.- June tide residuals (difference between 2015 and 2014) for the tide gauges of Data Posorja, Puna and Libertador Bolivar. Source: Author's elaboration.

From the tidal residuals obtained for each tide station, the percentage of time of each month in which positive residuals were present, which are indicators of higher tides in 2015 compared to 2014, was calculated. Thus, 100% represents the total time of each month, which corresponds to approximately 15 days as explained above. Thus, the following figure 4.3 shows that in April of the dry season the percentage of time in which

higher tides were presented in 2014 was slightly higher compared to 2015 in Data Posorja and Puna, while in Puerto Bolivar the percentage of time in which the highest tides occurred in 2014 was the same as in 2015.

In June, on the contrary, the percentages indicate that most of the time the tides were higher in 2015. For example, in Data Posorja and Puerto Bolivar more than 70% of the time in June the tide was higher in the 2015. In this way it was evidenced that, between April and June, it was in the month of June when there was a greater predominance in the time of higher tides in 2015 with El Niño conditions than in the 2014 normal year.
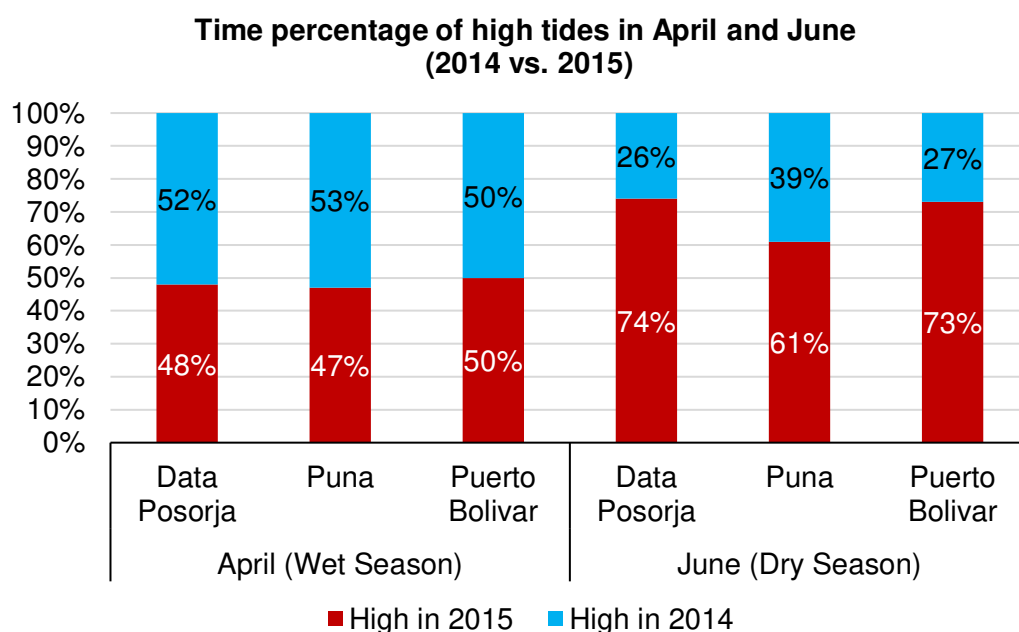
Figure 4.3.- Time percentage of high tides in April and June (2014 vs. 2015) for each tide gauge. Source: Author's elaboration.

4.2. Tides during wet season: April 2014 (Normal conditions) and April 2015 (El Niño conditions)

4.2.1. Spring tide during full moon

When analyzing the tide conditions of the month of April 2014 and 2015 in new moon, day corresponding to the period of spring tides, it was observed that the tides were higher with respect to the MSL in 2015. The difference was more evident during the high tide of both dates (Figure 4.4C and 4.5C). For example, in the April 2015 high tide (Figure 4.4C) the tides exceeded a height of 1.7 m in the southern area of the Jambeli Channel, the Morro Channel and along the Estero Salado, reaching maximum values estimated between 1.75 m and 1.85 m according to the color scale of the maps. Conversely, in 2014, in the areas mentioned above the tides were lower reaching approximately 1.6 m

in height (Figure 4.5C). Therefore, in 2015, El Niño year, there was an increase in tidal height estimated at 15 cm - 25 cm in these areas.

Furthermore, during the high tide in the Cascajal Channel the tide height between the east and west of the section is very different especially in 2015. In 2014, the tide in Cascajal reached heights between 1.25 m to the west and 1.5 m to the east, in general the difference was not very marked along the channel. The opposite happens in 2015, since to the east of Cascajal the level of the tides was approximately 1.6 m and west of the channel between 1 m and 1.25 m above the MSL. This difference in tidal height at both ends of the Cascajal Channel is due to the time it takes to reach the high tide towards the interior of the Gulf. Through the Morro Channel, the tide first reaches the Cascajal Channel through the Jambeli Channel [11], hence, the high tide arrives first at the Estero Salado than at the Guayas River and consequently to the east of the Cascajal Channel the tide will be greater than to the west, in the same moment of time close to high tide.

As the tidal wave continues to enter the Guayas River area, in 2015 they reached heights between 1.7 m and 2.8 m at the north of the channel and towards the interior of the modeled area of the Guayas River (Figure 4.4D). However, in 2014, maximum tides in the same areas of the Gulf were found in a range of 1.5 m to 2.4 m in height (Figure 4.5D). Consequently, there was a difference in height estimated between 20 cm and 40 cm between 2014 and 2015, being higher in this last year.

As low tide approached, in April 2015 there was an intensification of the lowest tides compared to April 2014 south of the Jambeli Channel and the Morro Channel. In 2015, the lowest tides reached values between 1 m and 1.5 m below the MSL in both channels (Figure 4.4 F), while in 2014 the level decreased to 0.25 m and 1.25 m with respect to the same reference level (Figure 4.5 F). At the same time, towards the interior of the Guayas River the tides were lower in 2014 compared to 2015, in other words, in 2015 the water level in this area during the low tide was at a higher height above of the MSL than in 2014.

Lunar phase: New Moon (April 18, 2015)

Figure 4.4.- New moon spring tide (18-Apr-2015) and tide time-series (Cyan: tides in A, Blue: Tides in B, Magenta: Tides in C – High Tide, Red: Tides in D, Yellow: Tides in E, Green: Tides in F – Low tide). Source: Author's elaboration.

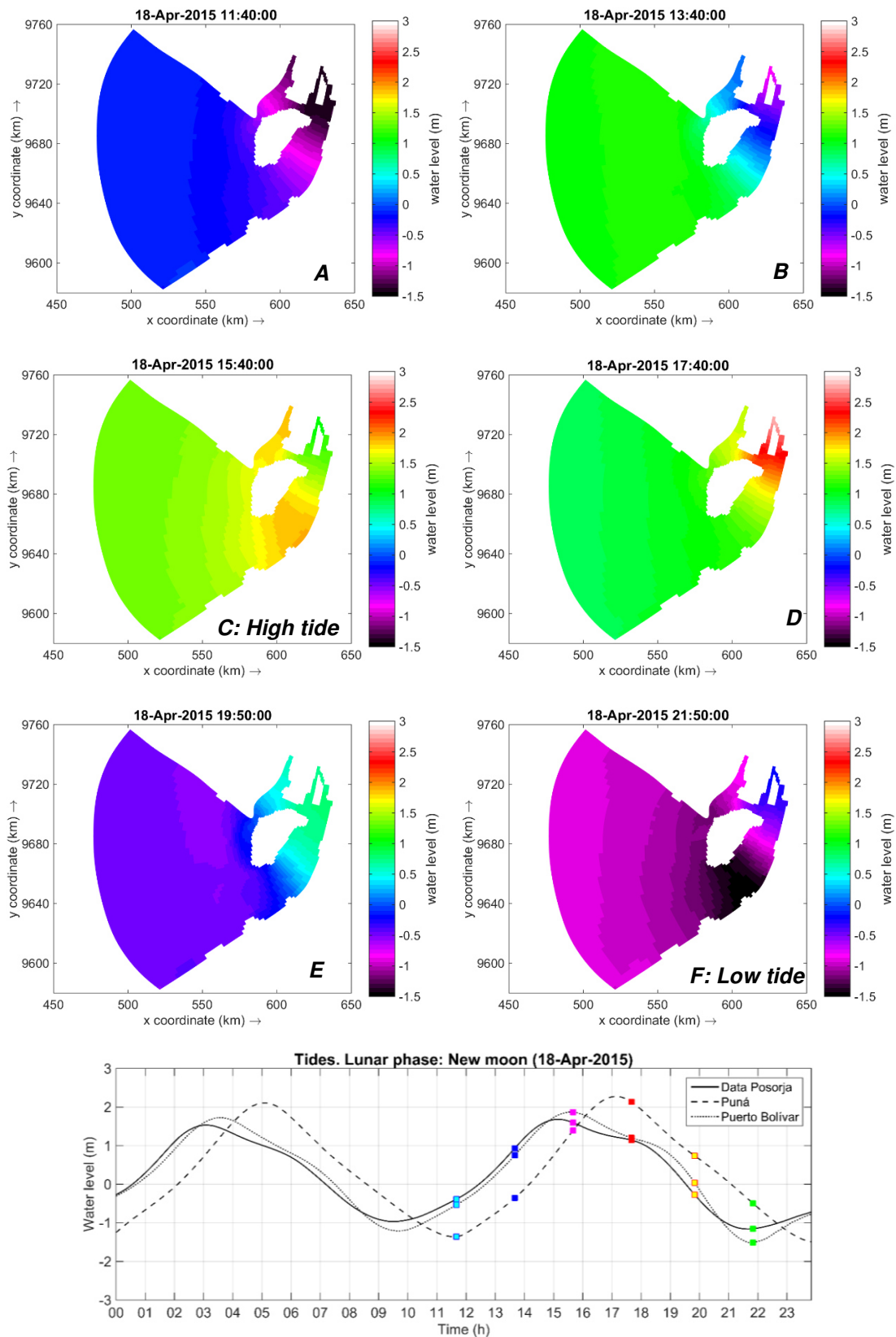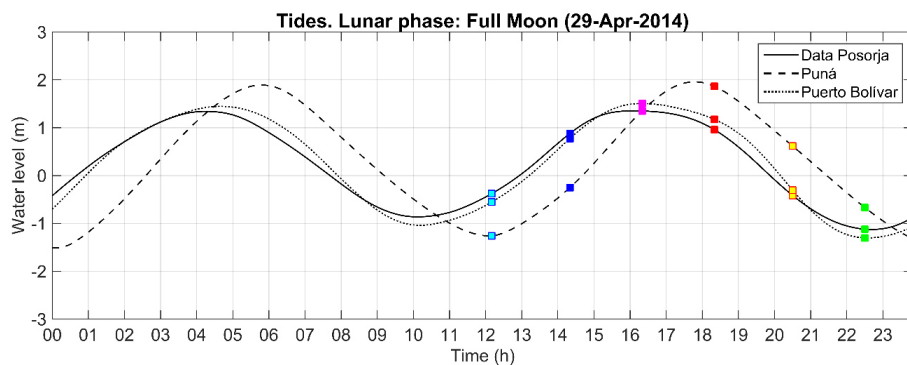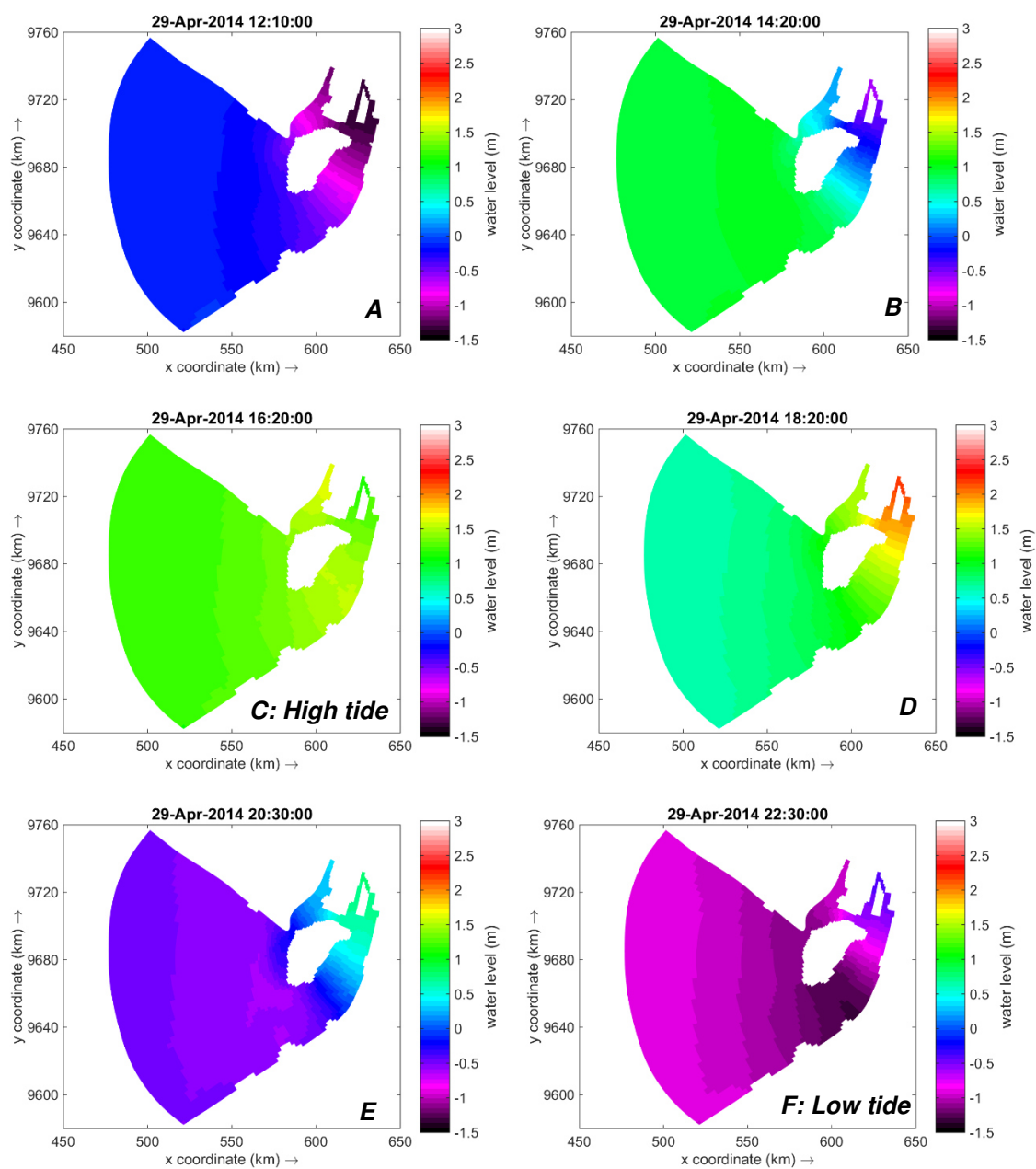**Lunar phase: New Moon (April 29, 2014)**

Figure 4.5.- New moon spring tide (29-Apr-2014) and tide time-series (Cyan: tides in A, Blue: Tides in B, Magenta: Tides in C – High Tide, Red: Tides in D, Yellow: Tides in E, Green: Tides in F – Low tide). Source: Author's elaboration.

4.2.1. Neap tide during first quarter

When comparing the results of the simulation of the month of April of the years 2014 and 2015 for a quadrature day, it was found that the tides presented a greater height in the whole area of the Gulf in 2015. As the tidal wave was advancing towards the interior of the Gulf it was observed, before the occurrence of the high tide in Jambeli, that the height of the tides in 2015 (Figure 4.6B) was approximately 25 cm higher than in 2014 from Data Posorja and Puerto Bolivar towards the sea (Figure 4.7B). This is because, in 2015, the water level was 0.75 m above the MSL and in 2014 it was 0.25 m above the MSL.

When the high tide occurred in the area of Jambeli near Puerto Bolivar, the tides in 2015 had an approximate height of 1 m from the outer limit of the Gulf and increased towards its interior, reaching values between 1.3 m and 1.4 m in the Jambeli Channel and Estero Salado (Figure 4.6C). Meanwhile, in 2014 the heights were lower (Figure 4.7C). From the outside of the Gulf, the estimated water level was 0.7 m, without exceeding 1 m in height with respect to the MSL from the Morro Channel and the Jambeli Channel to the interior of the estuary. In Cascajal, a small increase in water level was observed in 2015, however, not very significant compared to the rest of the Gulf. As already indicated, this may be due to the lack of a higher resolution of the grid used in Cascajal.

As the tide continued to enter the interior of the Gulf (Figures 4.6D and 4.7D), there was evidence of a decrease in water level towards the sea and its increase towards the mainland as usual. When the high tide reached the interior estuary, the water level was higher in 2015. Downstream from the river the tide reached heights in a range of 1.7 m - 2.1 m and along the Estero Salado 1 m in 2015 (Figure 4.6 D). In contrast, in 2014 the height of the tide from El Morro to Estero Salado increased from 0.75 m to less than 1 m and in the Guayas River between 1 m and 1.20 m in height (Figure 4.7D).

After the high tide, as the water level decreased, the tide height remained higher in 2015. During the low tide of both years (Figures 4.6F and 4.7F) in quadrature, as occurred during the syzygy, there was an intensification of the lowest tides, however, in 2015 occurred in a much smaller area of the Jambeli Channel. At the same time, in Estero Salado, no great differences were observed in the heights of the levels between 2014 and 2015. However, downstream from the Guayas River, the height of the water level was slightly higher in 2015, although in both years the level was below the NMM for being at low tide.

Lunar phase: First Quarter (April 25, 2015)

Figure 4.6.- First Quarter neap tide (25-Apr-2015) and tide time-series (Cyan: tides in A, Blue: Tides in B, Magenta: Tides in C – High Tide, Red: Tides in D, Yellow: Tides in E, Green: Tides in F – Low tide). Source: Author's elaboration.
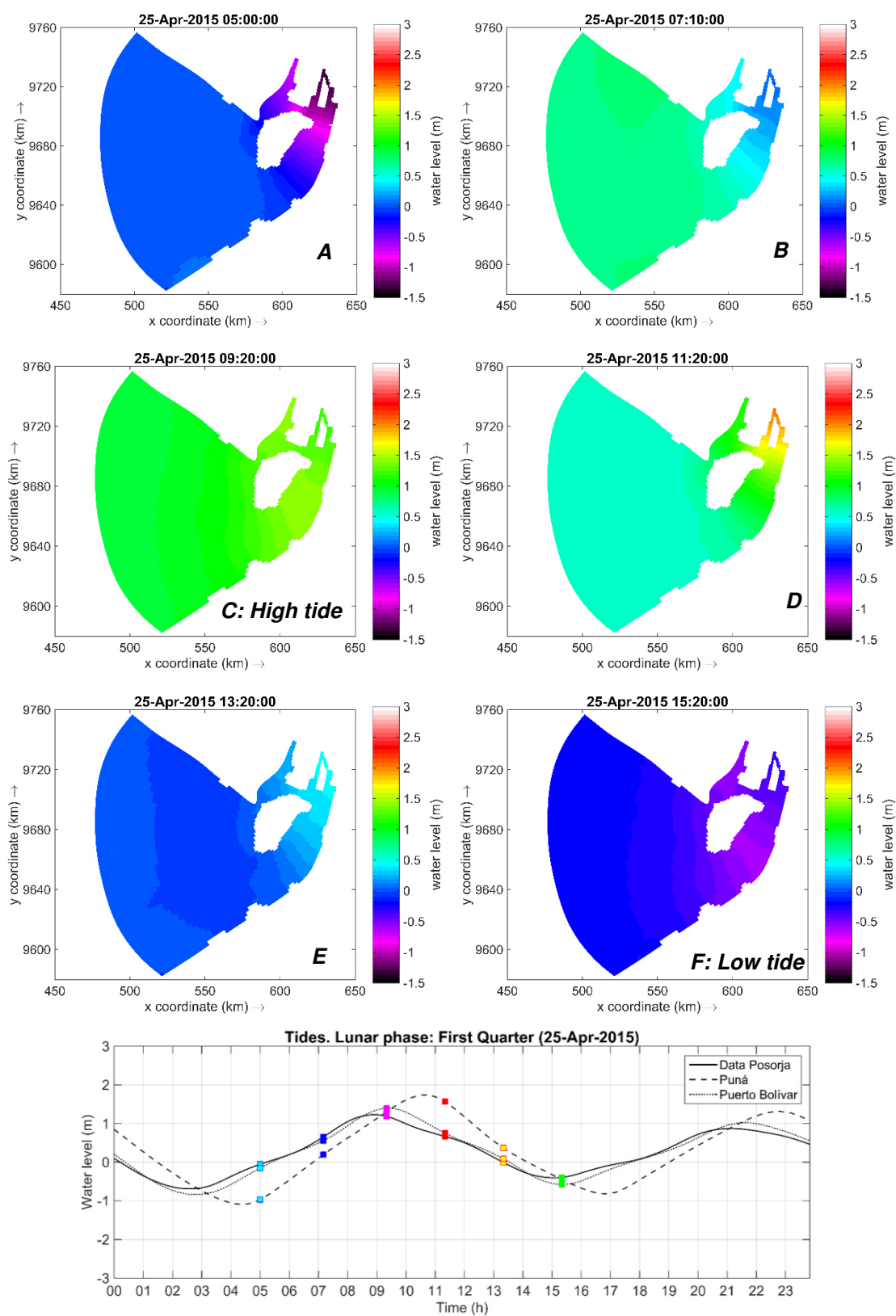
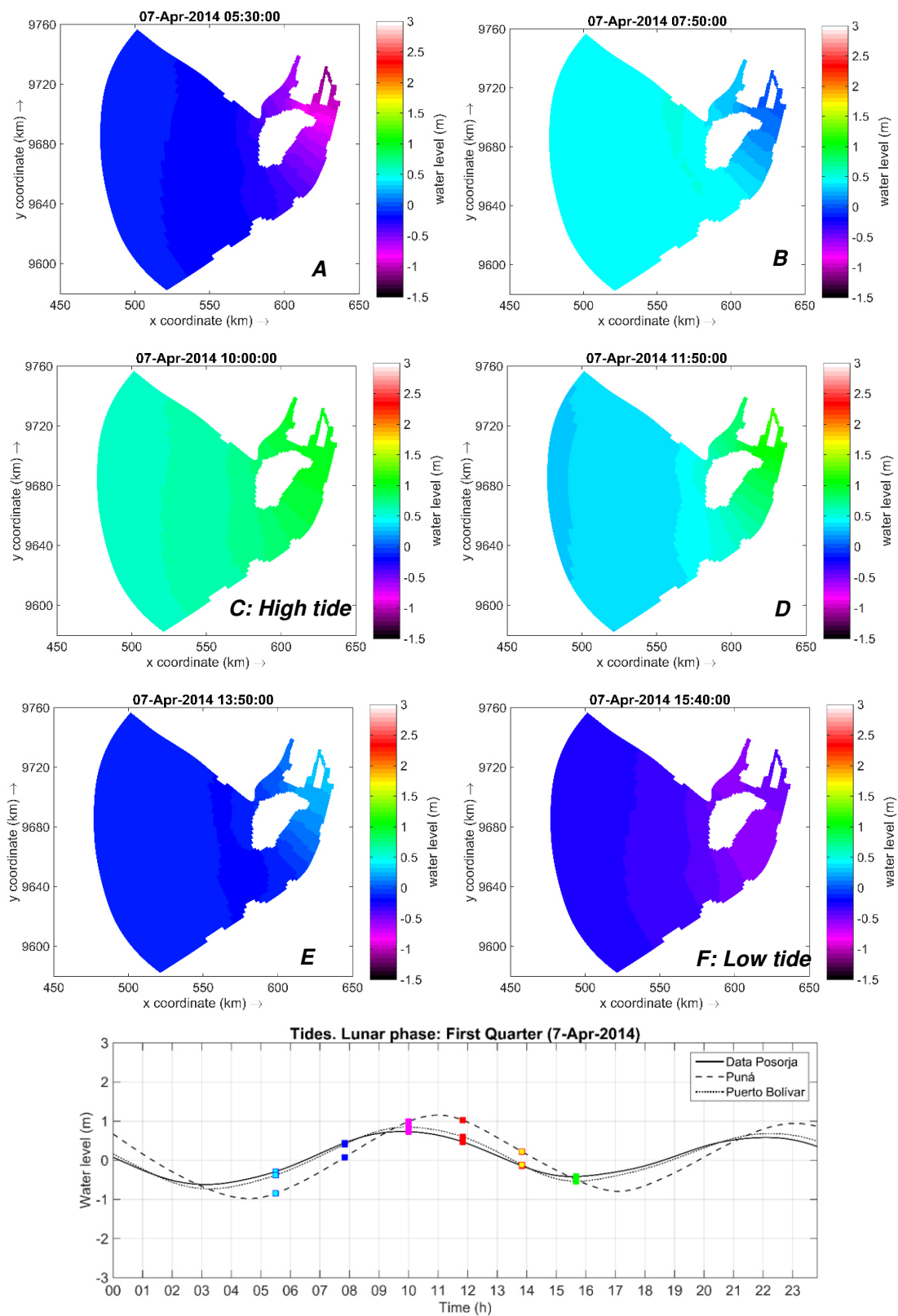**Lunar phase: First Quarter (April 7, 2014)**

Figure 4.7.- First Quarter neap tide (7-Apr-2014) and tide time-series (Cyan: tides in A, Blue: Tides in B, Magenta: Tides in C – High Tide, Red: Tides in D, Yellow: Tides in E, Green: Tides in F – Low tide). Source: Author's elaboration.

4.3. Tides during dry season: June 2014 (Normal conditions) and June 2015 (El Niño conditions)

Because the tides were lower in the month of June, the color scale was reduced to values between -1.5 m and 2 m in order to appreciate in more detail the variations in water level in the Gulf.

4.3.1. Spring tide during full moon

In the month of June during syzygy, significant differences were observed in the tide levels reached between 2014 and 2015. As the tidal wave propagated into the interior of the Gulf, it was observed that the height of the water level with respect to The NMM was higher in 2015. In 2015, an estimated height of 0.8 m was found from the outer limit of the study area to the south of Puna Island (Figure 4.8B). This height increased to the area of the Guayas River, in such a way that in 2015 the tide was approximately between 25 cm and 30 cm above the tide level of 2014 (Figure 4.9B).

In the month of June during syzygy, significant differences were observed in the tide levels reached between 2014 and 2015. As the tidal wave propagated into the interior of the Gulf, it was observed that the height of the water level with respect to The NMM was higher in 2015. In 2015, an estimated height of 0.8 m was found from the outer limit of the study area to the south of Puna Island (Figure 4.8B). This height increased to the area of the Guayas River, as a result, in 2015 the tide was approximately between 25 cm and 30 cm above the tide level of 2014 (Figure 4.9B).

At low tide south of the Jambeli Channel, the tide continued to grow with values close to 2 m in the innermost area of the Gulf, north of Mondragon Island. In June 2015 (Figure 4.8D) the water level was higher with respect to the MSL compared to 2014 downstream of the river (Figure 4.9D). During the low tide, outside the Gulf, the level of low tides intensified in June 2014 from the outer limit of the study area to the interior of the Estero Salado and the Jambeli Channel.

For example, in 2015, near the outer limit of the Gulf, the estimated height of the tide was -0.75 m (Figure 4.8F) and in 2014 it was -0.9 m with respect to the MSL (Figure 4.9F). In the same figures it was observed that in the north of the Morro Channel and in the southern area of the Jambeli Channel, the water level was -1.4 m with respect to the MSL in 2015, while in 2014 values close to -1.3 m and -1.35 m. At the mouth of the Guayas River the tides were lowest in 2015 at -1 m and in 2014 at -0.75 m approximately at low tide.

Lunar phase: Full Moon (June 2, 2015)

Figure 4.8.- New moon spring tide (2-Jun-2015) and tide time-series (Cyan: tides in A, Blue: Tides in B, Magenta: Tides in C – High Tide, Red: Tides in D, Yellow: Tides in E, Green: Tides in F – Low tide). Source: Author's elaboration.

Lunar phase: Full Moon (June 12, 2014)

Figure 4.9.- New moon spring tide (12-Jun-2014) and tide time-series (Cyan: tides in A, Blue: Tides in B, Magenta: Tides in C – High Tide, Red: Tides in D, Yellow: Tides in E, Green: Tides in F – Low tide). Source: Author's elaboration.

4.3.2. Neap tide during first quarter

In quadrature during the month of June 2015, the tidal wave entered the Gulf with a greater height compared to 2014. In 2015, the wave propagated from the outer zone of the Gulf with 0.25 m in height (Figure 4.10A) and in 2014 with values close to 0 m with respect to the MSL (Figure 4.11A). While the wave continued to enter the study area, the height of the tide increased throughout the Gulf to values higher than 0.5 m in 2015. In 2014, the same happened except for the area downstream of the river where the water level was very close to the MSL. Between both years the difference in height in this area was about 50 cm more in 2015 than in 2014.

When the high tide occurred, the difference in tidal height between both years was significant. In 2015 the tide in the Jambeli Channel was found between 1.1 m to the south and 1.4 m to the north, on the other hand, in the Morro Channel the height was approximately 1.1 m and in the Estero Salado it was slightly higher with heights between 1.2 m to the south and 1.35 m to the north. Similarly, from the west of the Cascajal Channel to the north of Mondragon Island in the Guayas River, the estimated tide height was 1.5 m in 2015 (Figure 4.10C).

On the other hand, in 2014 the height of the tides from the south of the Jambeli Channel to the north of the Mondragon Island was between 0.9 m and 1.2 m. Likewise, from the Morro Channel to the north of the Estero Salado, the estimated height of the tide presented values between 1 m and 1.3 m (Figure 4.11C). In the quadrature of June, the differences between the low tides were not very marked, in both years the level reached approximately 0.5 m below the MSL, although in 2015 the tidal height in the outer zone of the Gulf was slightly higher than in the 2014 (figure 4.10F and 4.11F).

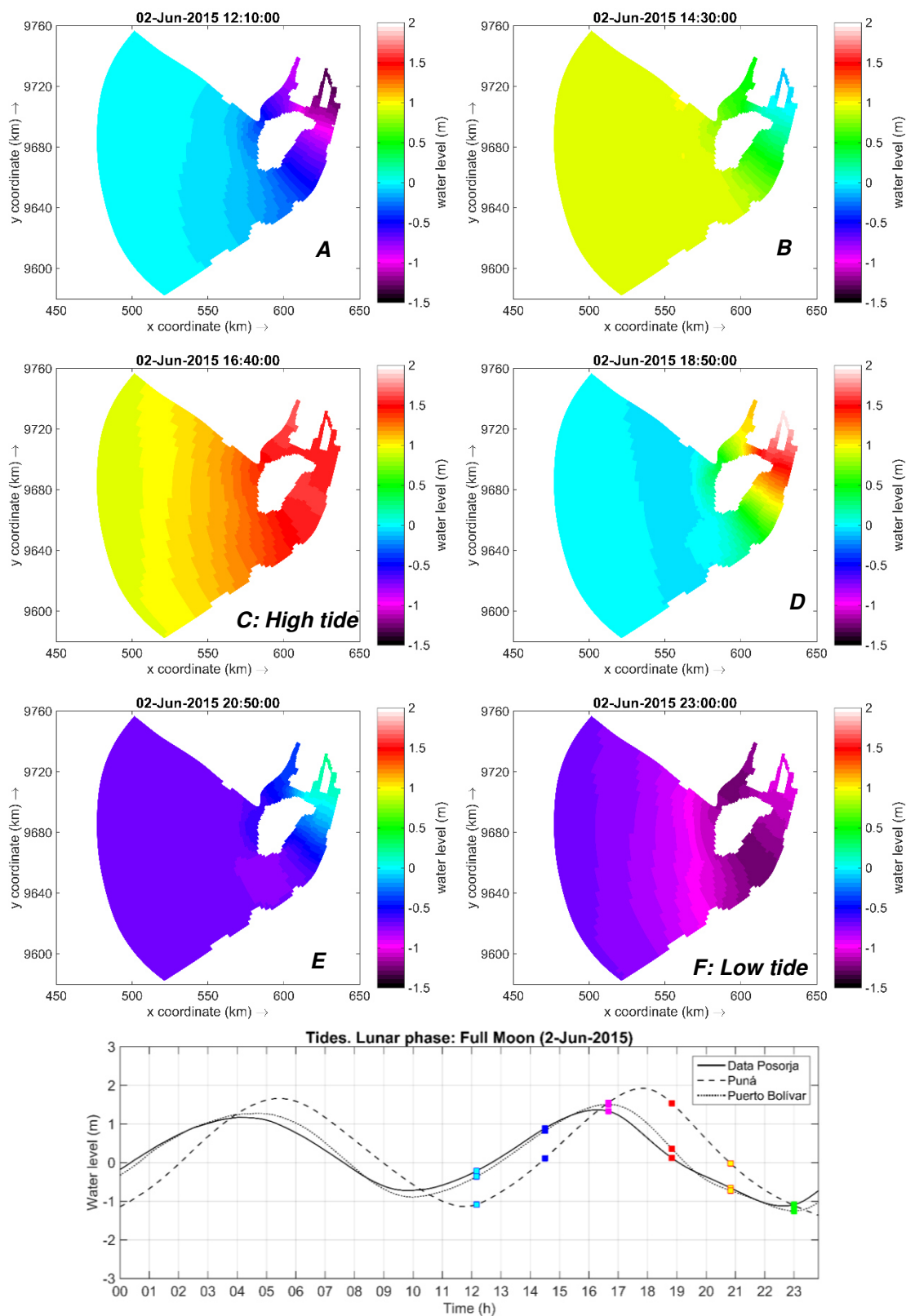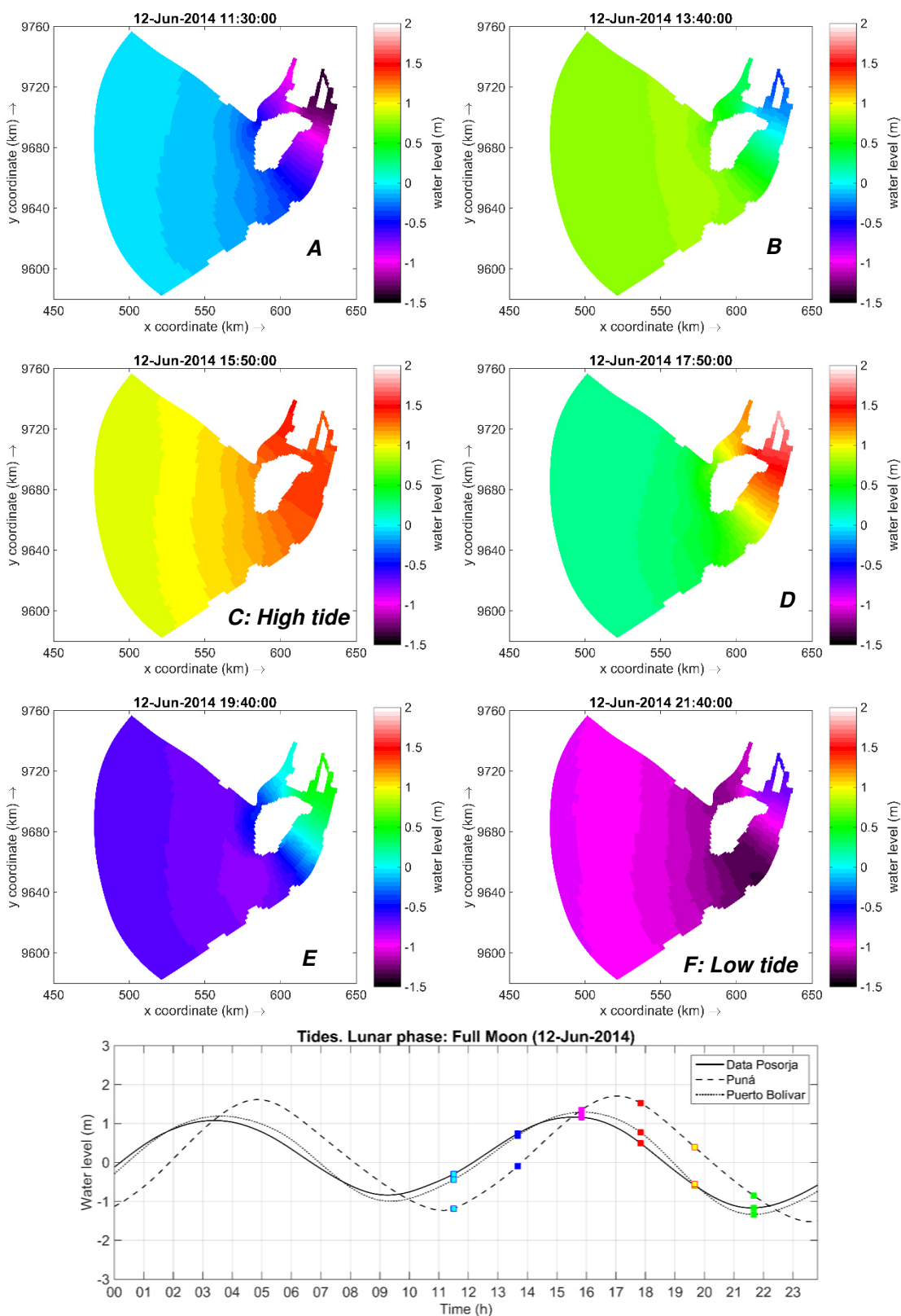**Lunar phase: First Quarter (June 24, 2015)**

Figure 4.10.- New moon spring tide (24-Jun-2015) and tide time-series (Cyan: tides in A, Blue: Tides in B, Magenta: Tides in C – High Tide, Red: Tides in D, Yellow: Tides in E, Green: Tides in F – Low tide). Source: Author's elaboration.
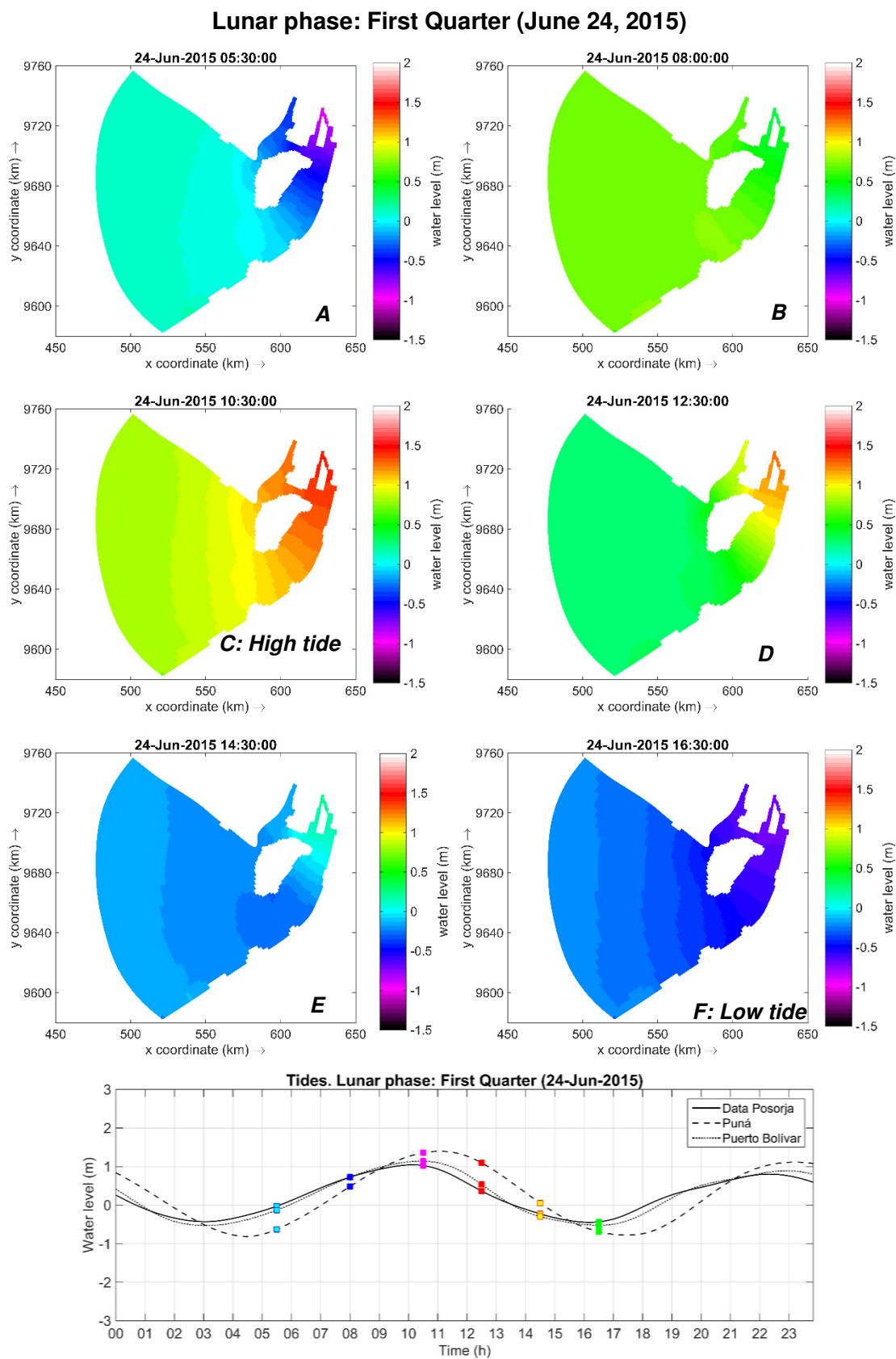
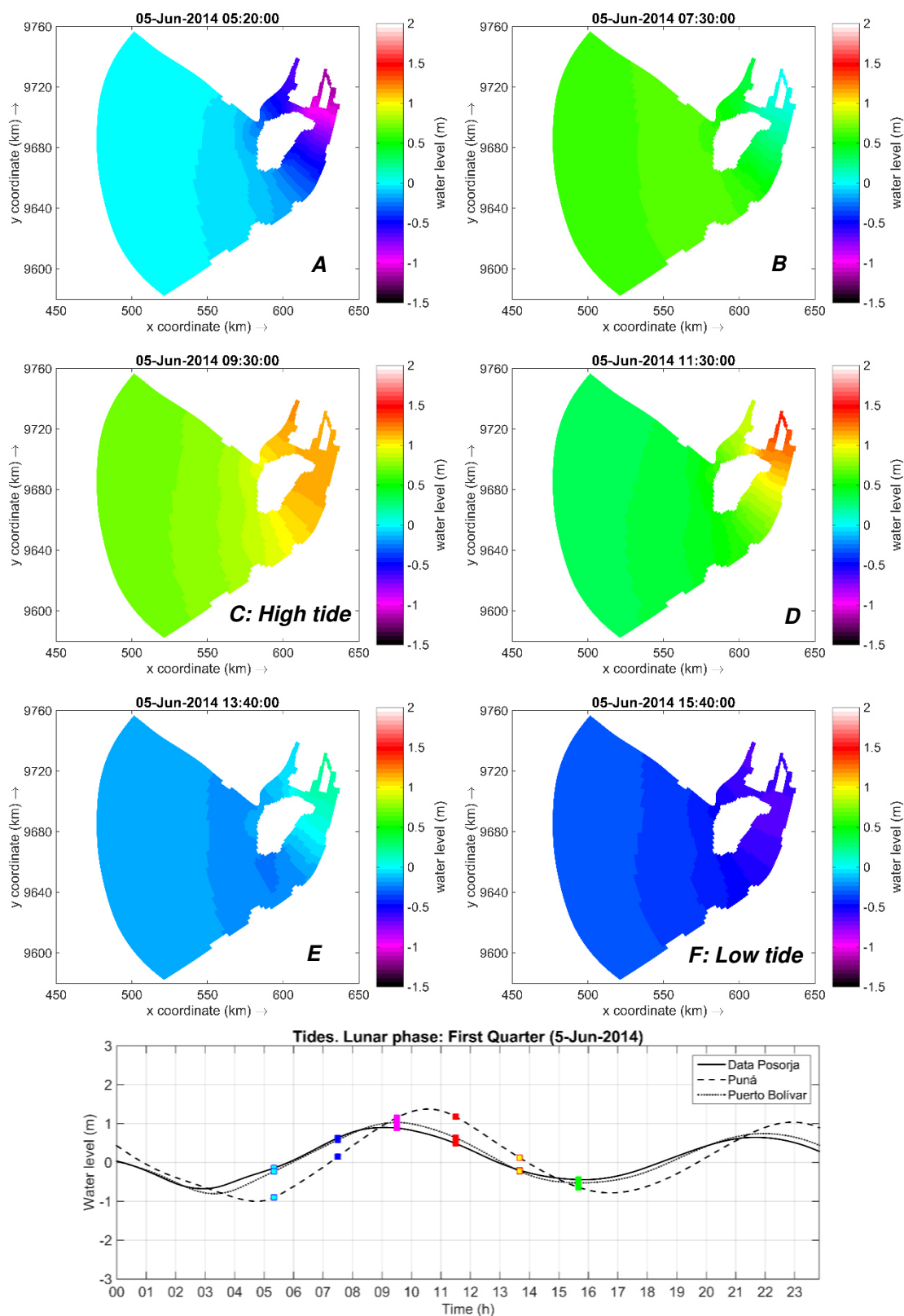**Lunar phase: First Quarter (June 5, 2014)**

Figure 4.11.- New moon spring tide (5-Jun-2014) and tide time-series (Cyan: tides in A, Blue: Tides in B, Magenta: Tides in C – High Tide, Red: Tides in D, Yellow: Tides in E, Green: Tides in F – Low tide). Source: Author's elaboration.

In general, it was evident during the compared dates that the high tides were higher in 2015 compared to 2014 in the whole modeled zone of the Gulf. This occurred in both syzygy and quadrature for the months of April and June that have been compared in this study. The elevation of the tides was more evident in the Jambeli Channel and the Morro Channel, as well as in the innermost zone of the Gulf, in the Estero Salado and downstream of the Guayas River. However, the behavior of the tides between Estero Salado and Guayas River is associated to two different conditions as indicated in [7], in the first one it is of stationary type and in the second progressive one.

During the low tide the minimum tide levels intensified in 2015 with respect to 2014 in the month of April. On the contrary, during the June spring tide, an intensification of the lowest tides was observed in 2014 in relation to the year 2015. However, that level difference in the low tides of both years was not very high. In the same way, during the quadrature no significant differences were observed between the low waters of both years, since in 2015 and 2014 the lowest tides were very close to 0.5 m below the MSL.

Additionally, the difference in the water level between the month of April corresponding to the wet season and the month of June belonging to the dry season was evident since in April the height of the tide was greater in both years. When analyzing these periods of time, the seasonal difference in the water level between both months is clearly identified, especially in the area downstream of the Guayas River, since it is the main source of fresh water in the Gulf. During the wet season, rainfall is more frequent and intense, generating higher flows that discharge into the Gulf mainly through the Guayas River. Therefore, it is verified that seasonality is a factor that causes significant changes in the Gulf as indicated in [1], [4].

However, it is important to consider that when performing the simulation using the tides measured by the tide gauges, the effect of the flows of large freshwater contributors such as the Guayas River is implicitly considered. If the contribution of flows were added to the model, the effect of the discharge would be doubled. Therefore, although it is possible to show the difference in the height of the water level due to seasonality, it is not possible to show that the difference in height of the tide between an El Niño year and a normal year for the same months of study, it is related in greater or lesser magnitude to the flows. Since this may also be a consequence of other meteorological factors during a El Niño year.

In addition, although the tide levels were higher in 2015 when El Niño conditions existed, it is required to verify that this is indeed the influence of this phenomenon. Since as indicated [7], the tidal constituents have a direct relationship with the variation in water

reference levels. Therefore, it is possible that within this height at the water level of 2015 there will be a greater influence of the tidal constituents than the rise in sea level due to an El Niño event. Additionally, near the coast, the Gulf circulation is also influenced by factors such as: horizontal and vertical friction, local accelerations that occur in the water, effects of wind force and resonant fluxes, which are due to the morphology of the area [1], which have not been analyzed in depth in this project.

On the other hand, the morphology of the Gulf of Guayaquil plays an important role in the amplification of tides as explained in Chapter 1. In all the dates analyzed it was observed that as the tidal wave propagates into the estuary its magnitude increases, since when entering, it moves through increasingly narrow channels such as the Morro Channel, Jambeli Channel and Cascajal Channel. This happens in estuaries or bays as described [10]. Consequently, when arriving to narrower areas such as the Estero Salado and the Guayas River, the tides are amplified in comparison to the tides in the outer zone of the Gulf.

Additionally, the results of the model allowed to verify that the tide always enters first through the Morro Channel and then through the Jambeli Channel, as mentioned by Chavarría in 1988 [7]. In relation to this, it was evidenced in all the cases that the high tide arrives first at the area of Estero Salado and then at the Guayas River. This pattern was repeated independently of the lunar phase and the presence of the El Niño 2015-2016 event in the months of June and April.

4.4. Velocities

This section shows a few results from another application of the Delft3D model as the magnitude of the tidal currents in the study area. The complete analysis of the magnitude and direction of the currents can help to understand the movement of the sediments and their deposit in the sites that are a threat to the safe navigation of the vessels due to the presence of bathymetric lows or sediment bars. Similarly, it can contribute to the study of pollutant transport and water renewal in the Gulf in conjunction with tidal results.

4.5. Velocities in April 2014 and April 2015

Between April 2014 and 2015 the velocities were higher in 2015 on the dates corresponding to the lunar phase of the new moon where the syzygies occur. In 2015 during the flood tide the velocity was found in a range of 50 cm/s and 80 cm/s along the Jambeli Channel and Morro Channel up to Cascajal (Figure 4.12A). On the contrary, in ebb tides the maximum velocities reached more than 1 m/s in both channels (Figure 4.12C). In the middle of the cycle, the velocities did not exceed 60 cm/s in the Jambeli Channel, except for certain specific areas where they reached approximately 75 cm/s.

In the Morro Channel and Cascajal, higher velocities of up to 80 cm/s occurred (Figure 4.12B).

Figure 4.12.- Flow velocity during new moon spring tide (18-Apr-2015) at high tide (A), mid-low tide (B), low tide (C). Source: Author's elaboration.

In 2014, during the flood tide the velocities registered in the Jambeli Channel were between 50 cm/s and 75 cm/s without covering the entire width of the channel to the south (Figure 4.13A). At the same time, in El Morro the flow was displaced at an estimated velocity of 75 cm/s through a marked line to the west of the channel reaching Cascajal. At ebb tide, velocities were higher reaching maximums of approximately 90 cm/s at the south of the Jambeli Channel and in the Morro Channel (Figure 4.13C). In the middle of the cycle, the values reached an estimated maximum of 1.7 m/s in the Morro Channel. Additionally, the velocities before reaching the mentioned channel were between 50 cm/s and 75 cm/s (Figure 4.13B).

Figure 4.13.- Flow velocity during new moon spring tide (29-Apr-2014) at high tide (A), mid-low tide (B), low tide (C). Source: Author's elaboration.

4.6. Velocities in June 2014 and June 2015

In June of 2015 it was observed that between the flood and ebb tide the higher velocities were in the ebb tide, although the difference was not as marked as in April during the wet season. In both tidal states, the velocities were approximately of 60 cm/s (Figure 4.14 A, C), the main difference being the area that presented these values. At ebb tide, these velocities were found much closer to the southern end and spread uniformly to the north, unlike what occurred in flood tide (Figure 4.14C).

In the middle of the cycle the highest velocities were recorded, exceeding 1 m/s in the Morro Channel and the Jambeli Channel. From the southern end of the Jambeli Channel, velocities were found between 60 cm/s to 1 m/s to the north, with an area of maximum velocities along the east of the channel in front of Puerto Bolivar of approximately 1.75 m/s. This value was also found in El Morro (Figure 4.14B).
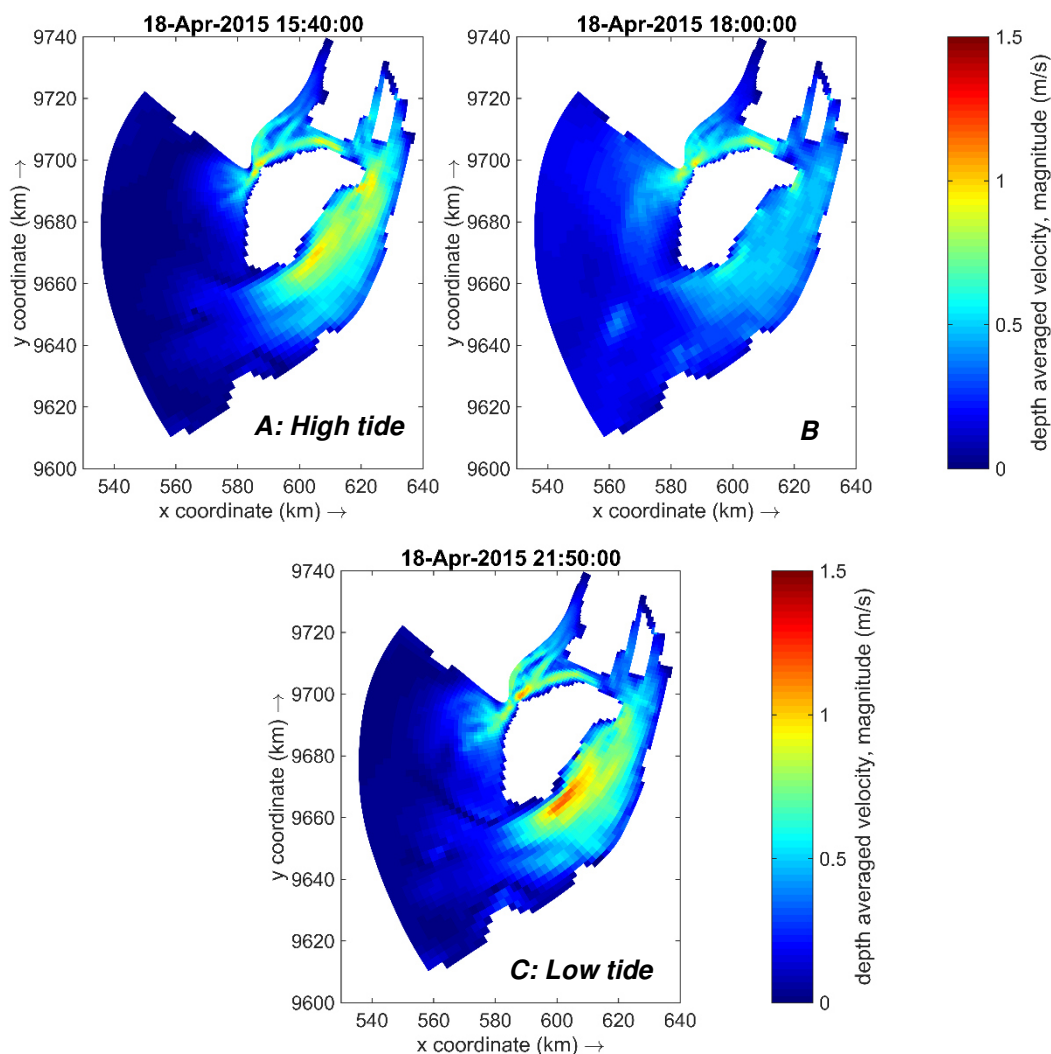
Figure 4.14.- Flow velocity during full moon spring tide (2-Jun-2015) at high tide (A), mid-low tide (B), low tide (C). Source: Author's elaboration.

In June 2014, the velocities were also higher in ebb tides than during the flood tides. In flood tides, the maximum recorded velocity was approximately 60 cm/s in the Jambeli Channel, Cascajal Channel and Morro Channel (Figure 4.15A). Conversely, at reflux velocities reached an estimated 90 cm/s in the same areas, especially in Jambeli (Figure 4.15C). At mid-cycle, velocities were in a range between 90 cm/s and 1.70 m/s at El Morro and on the east side of the Jambeli Channel in front of Puerto Bolivar (Figure 4.15B).
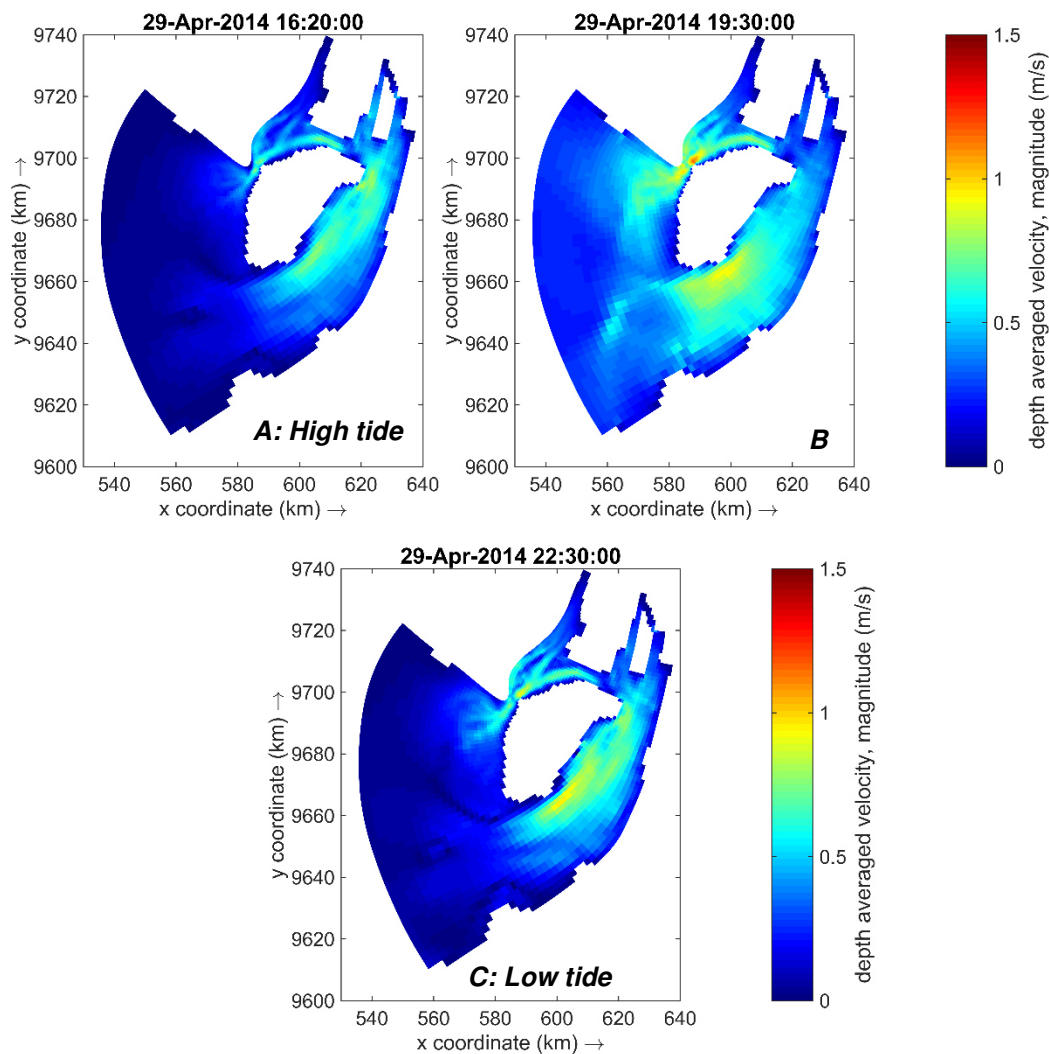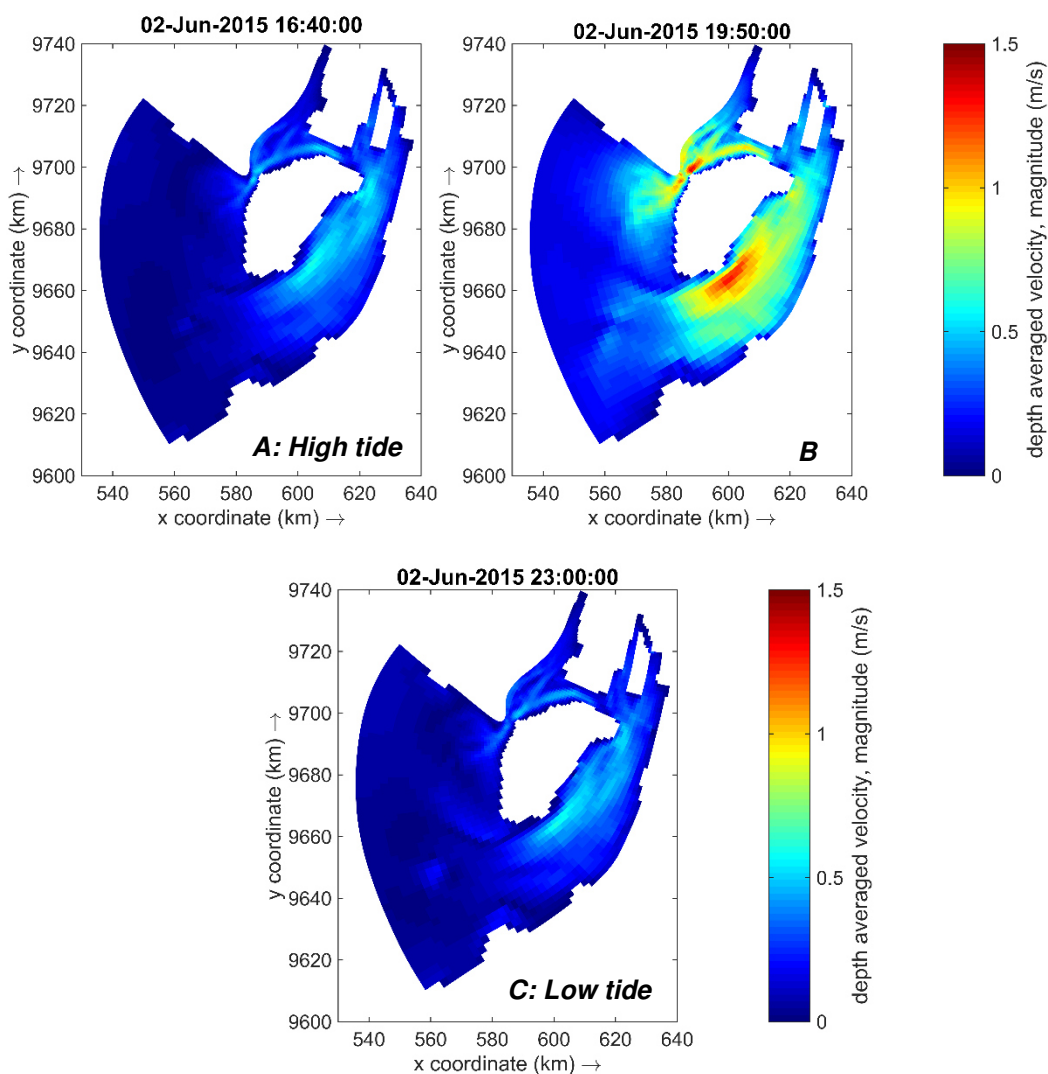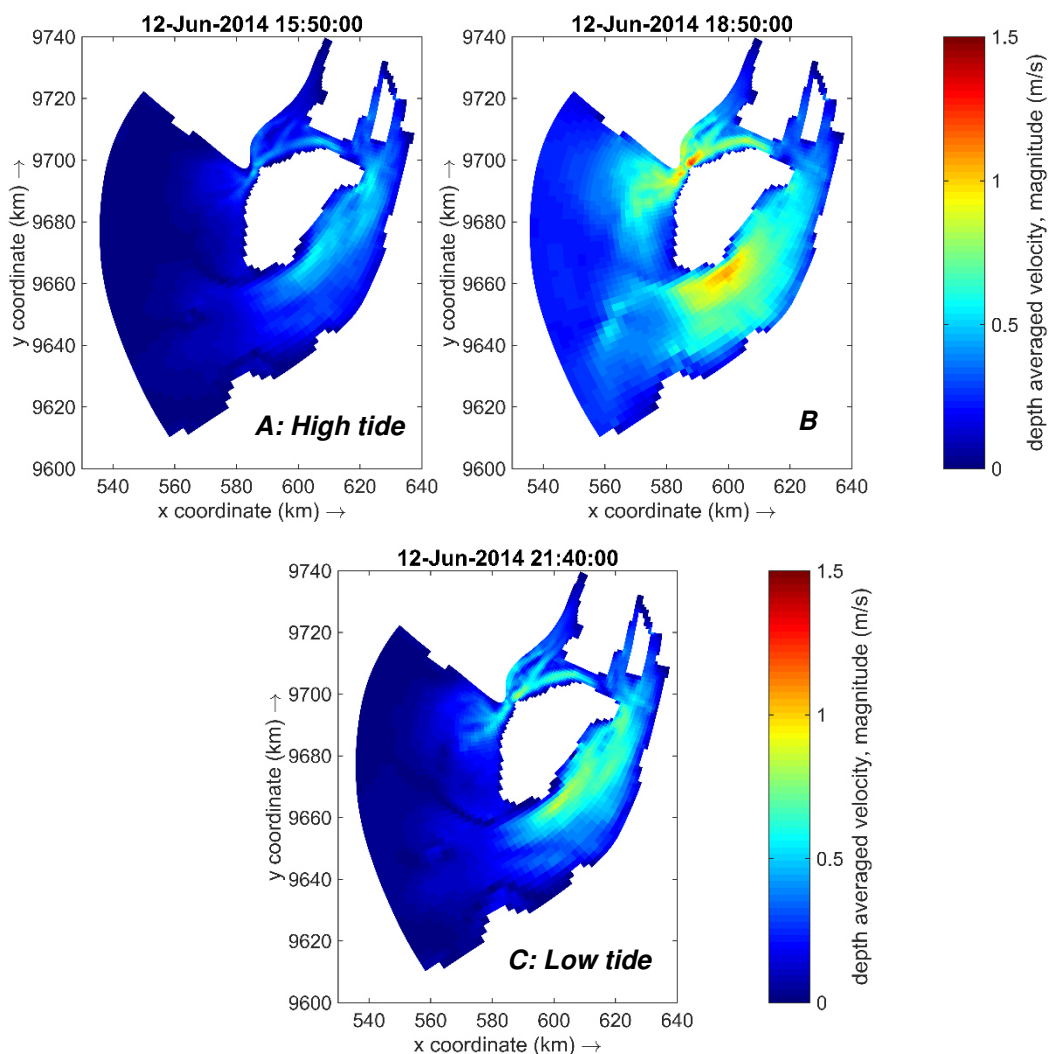
Figure 4.15.- Flow velocity during full moon spring tide (12-Jun-2014) at high tide (A), mid-low tide (B), low tide (C). Source: Author's elaboration.

In summary, the implementation of the model also allowed to obtain the velocity of the study area. As previous studies have reported [6], [9], [44], in the area of Estero Salado the velocities are higher in ebb tides than in flood tides. Most current velocity data have been registered with oceanographic measurement devices in specific stations of the Access Channel since it is the entrance route to the Guayaquil Maritime Port. However, with the results of the model it was possible to verify that this occurs in a wider area of the Gulf, being more evident in the main channels of the Gulf: Jambeli Channel, Morro Channel and Cascajal Channel.

Therefore, magnitude velocity was higher in ebb tides than in flood tides in the Gulf. This happened both in 2014 and 2015 and during the dry and wet seasons, consequently, it was evident that this is a normal and repetitive pattern in the study area in each tidal cycle and that it is not influenced by the presence of an El Niño event. However, the magnitude of the velocity was different between 2014 and 2015, being higher in April

and June 2015, probably due to the higher flows and rainfall recorded by INAMHI during that year (flow: April= 771 m³/s and June= 545 m³/s in the Daule La Capilla station, precipitation: April= 113 mm and June= 8 mm in the Guayaquil A. station) as a result of the influence of El Niño compared to the year 2014 (April= 192 m³/s and June= 304 m³/s at the Daule La Capilla station, precipitation: April= 312 mm and June= 36 mm) as indicated in Chapter 1.

Likewise, there were seasonal differences since it was found that in April 2014 and 2015 during the wet season there were higher velocities than in June 2014 and 2015 during the dry season. This is also because of greater contribution of fresh water to the Gulf due to more intense and frequent precipitation, as well as higher river flows that occurred in April of both years as explained above. Additionally, when comparing the velocity maps with the bathymetry, it was found that the highest velocities in the Gulf occured in the deepest zones. For this reason, the pattern of maximum velocities was repeated in the same areas in all cases.

4.7. Application of the model results in other study areas

The results of the model allowed to visualize the variation of the tide and the velocity in the whole Gulf generated from an open boundary condition that used the data from a single tide gauge. In addition, the validation of the results showed that the model represented water level very close to reality in the selected monitoring stations; even though the stations were located very close to the coast where it might be more difficult to obtain an optimal result since the tidal wave in that area is influenced by other processes and factors not discussed in this project. In Puna the results were not the most optimal according to what was explained in Chapter 3, however, as explained before, this could be solved with a finer grid in that area.

In this way, the implementation of the model can be considered a powerful tool to visualize variables such as the tide and current velocity, unlike other sources of information such as remote sensor data. Remote sensors do not always have the desired temporal and spatial resolution, also, in large inlets such as the Gulf of Guayaquil, obtaining data from remote sensors with the characteristics necessary for certain studies is generally difficult due to the temporal and spatial resolution available.

Water level rise sceneries

The application of the model in future climate research would allow to establish, according to the study objective, different scenarios of water level elevation in the Gulf and estuary. It has already been demonstrated during the calibration and validation stage of the model of the present work that the model reproduces the level of water in the Gulf

of Guayaquil in a very close way to the measured. In addition, physical parameters have been established to obtain optimal simulated results, which could serve as a guide for future hydrodynamic modeling in the Gulf. Therefore, this work demonstrates the potential application of this numerical tool to broaden the knowledge about possible consequences in the Gulf before scenarios of water level elevation due to climatic events such as El Niño or others. In this way, it could facilitate the identification of the coastal areas most vulnerable to flooding in the Gulf or to erosive processes that affect many structures and coastal ecosystems.

In fact, several studies on coastal floods have already been carried out in other countries with the application of the Delft3D model. For example, in the Shoalhaven Estuary in Australia the model was applied to determine the extent and depth of flooding due to a storm event [45]. Its application has also contributed to the study of impacts on tidal inlet or basin systems as a consequence of the sea level rise [46]. In other cases it has allowed modeling scenarios to investigate how the tide and floods have changed over time [47].

Navigation

The results of the tidal simulation can be useful and applicable in other topics of interest related to the Gulf. For example, in the Gulf of Guayaquil the study of tides is critical to navigation issues. Moving vessels in this area need to know conditions in certain dates and times, so that there are no problems during navigation. With the model it is possible to identify the areas where the water level becomes lower in the Gulf, especially in the Access Channel, and that consequently may cause inconveniences in the entry and exit of vessels.

This can be complemented with the visualization of the bathymetry in the model to identify bathymetry lows in the Gulf that could be a danger for ships due to grounding. With the construction of the new Deep-Water Port in Posorja, it is foreseen that ships of greater depth arrive, therefore, the use of numerical modeling tools such as the one applied in the present work, offers many advantages and facilities to carry out more complete studies on navigation in the Gulf.

Contamination

Using the results of the tidal simulation is also highly relevant in terms of pollution and water quality. It has been reported that large river discharges in conjunction with tidal exchange when there is low water residence time, allow to maintain good water quality [4]. Besides, tidal flushing contributes to the movement of pollutants [48].

The Gulf of Guayaquil faces problems of water pollution for several years due to the anthropogenic influence. Being an area of great ecological importance in the country, conducting studies on the transport of pollutants is necessary. In this context, the results of tides and current velocity of the model constitute a contribution that can serve as a basis for further studies of pollution in the Gulf.

Previous studies have shown the influence of tides on the transport of pollutants and on the quality of estuarine waters in the Gulf [49], [50]. The visualization of the current velocity in the Gulf with the simulated results facilitates the determination of areas where pollutants can be concentrated or dispersed more quickly. For example, these results could complement transport studies of persistent pollutants in the Gulf such as hydrocarbons, whose presence has been reported in areas such as Estero Salado in [50], [51].

Likewise, spatially visualizing the tide in the Gulf, even in the inner zone, at an acceptable temporal and spatial resolution helps determine the transport of different pollutants with the entry and exit of water. For example, the pollution plume can move to and from the coast with the tides as indicated in [52].

Water renewal time

The time of water renewal is a factor that estimates the time in which a certain percentage of water is replaced by an equal amount of fresh water [53]. In relation to this topic, another utility of the results of the model in terms of spatial visualization of the current velocity and behavior of the tides is in studies of the capacity of renewing the water of the Gulf. This would contribute to a more detailed understanding of how well the Gulf is capable of self-purging in the face of different contamination events; especially, considering that the dynamics of this ecosystem is influenced mainly by the tides and is also vulnerable to pollution events from different sources. Therefore, the study of the time of renewal of the Gulf water is fundamental to improve the management of this and expand the knowledge of the natural response of the ecosystem to pollution.

CONCLUSIONS AND RECOMMENDATIONS

Conclusions

1. Considering the whole series of data for each simulated month, it was found that, a higher percentage of time in June (> 70%), during the dry season, higher tides occurred in 2015 with El Niño conditions that 2014 under normal conditions at the stations of Puerto Bolivar, Data Posorja and Puna. The opposite happened in April of the wet season where a higher percentage of time occurred higher tides in 2014 (> 50%). Thus, in June 2015 there was a greater dominance of high tides than in April 2015.

2. Considering only the dates of spring and neap tides analyzed in the months of April and June, the height of the tide was greater in 2015 during El Niño, compared to 2014 during normal conditions. However, it cannot be said that this elevation is due only to the event El Niño 2015-2016, since as reported by INAMHI in [11] during this event, precipitation was not as intense as in past El Niño events such as the events of 1997 and 1982.

3. The influence of morphology on the tidal amplification in the inner area of the estuary was observed in narrow channels such as the Estero Salado and the mouth of the Guayas River where the tidal amplitude was greater.

4. The model could adequately represent the tides at the Data Posorja and Puerto Bolivar stations. In Puna the results of the calibration process were not as satisfactory, there being an approximately 50% adjustment between the observed and simulated data.

5. The utility offered by the model to visualize the behavior of the tide in the Gulf with an adequate spatial resolution was demonstrated, making possible its application in other topics of interest such as: water level scenarios, transport studies of pollutants, renewal of the water and navigation issues in the Gulf.

6. Additionally, although it was not an object of study, the results suggest that the presence of El Niño does not influence the variation of the height of the tides as it does seasonality.

7. Current velocity was higher in April and June 2015 compared to 2014, which may be associated with the increase in the flow of rivers discharging into the Gulf, mainly from the Guayas River, and more intense and frequent rainfall according to the data registered by INAMHI.

8. It was found that current velocity was higher at ebb tide than at flood tide and maximum at half the tidal cycle, except for April 2015. This velocity pattern was not affected or modified by the presence of an El Niño event or seasonality, since it occurred in both years.

9. Seasonality did influence the magnitude of current velocity. In April during the wet season the velocity of the currents was higher than in June of the dry season in 2014 and 2015.

10. Higher current velocities occur in the deepest areas of the Gulf.

Recommendations

1. Refine the grid in the inner zone of the estuary to have a better resolution in the narrowest channels such as Cascajal and obtain a better fit of the model between the observed and simulated data. In such a way, that the simulation results can represent the tidal conditions as close as measured.

2. Use more available stations with observed tidal data in the internal and external area of the estuary to calibrate and validate the model. With the objective of verifying that in internal zones such as the Estero Salado and the Guayas River, as well as in the middle of the outer Gulf in deep waters, the adjustment of the model is optimal.

3. Replicate the study with data from tides of past El Niño events, for example, the 1997-98 El Niño, to determine if similar conditions are repeated in the tides and at the velocities reported in this report.

4. Include different scenarios to identify if the height of the tides in the estuary is totally influenced by El Niño conditions or by other factors such as variations in the harmonic tidal constituents in the months studied. Likewise, include the effect of other variables such as winds and flow discharges of the main rivers of the estuary.

5. Include currents in the calibration and validation process of the model, using velocity data from different transects along the exterior and interior estuaries in order to verify how optimal the velocity results delivered by the model are.

REFERENCES

[1]   CIIFEN, "El Niño 2015-2016: evolución, vulnerabilidad e impactos en Latinoamérica," 2017.

[2]   E. Zambrano, "El Fénomeno de 'El Niño' y la Oscilación del Sur (ENSO)," *Acta Oceanográfica del Pacífico*, vol. 3, no. 1. INOCAR, 1986.

[3]   A. Doherty, "Elevated Sea Levels During 2015-2016 Strong El Niño," 2015.

[4]   J. G. Stenfert, R. M. Rubaij Bouman, R. C. Tutein Nolthenius, and S. Joosten, "Flood Risk Guayaquil: A critical analysis on inundations," 2017.

[5]   R. H. Stewart, *Introduction to Physical Oceanography*. Texas A & M University, 2008.

[6]   Asociación Geoestudios and Consulsua, "Puerto Marítimo de Guayaquil. FASE II - Capítulo 7. Condiciones Hidrodinámicas del Canal de Acceso.," Guayaquil, Ecuador, 2012.

[7]   M. R. Stevenson, "Variaciones estacionales en el Golfo de Guayaquil, un estuario tropical," *Instituto Nacional de Pesca. Boletín Científico y Técnico.*, vol. 4, no. 1, Guayaquil, Ecuador, p. 133, Dec-1981.

[8]   R. R. Twilley, W. Cárdenas, V. . Rivera, J. Espinoza, R. Suescum, M. Armijos, and L. Solórzano, "The Gulf of Guayaquil and the Guayas River Estuary, Ecuador," in *Coastal Marine Ecosystems of Latin America. Ecological Studies (Analysis and Synthesis)*, vol. 144, no. January, U. Seeliger and B. Kjerfve, Eds. Springer, Berlin, Heidelberg, 2001, pp. 245–263.

[9]   Centro de Estudios del Medio Ambiente (CEMA), "Informe de monitoreo ambiental del dragado de mantenimiento del canal de acceso al Puerto Marítimo de Guayaquil," Guayaquil, Ecuador, 2009.

[10]   National Oceanic and Atmospheric Administration (NOAA), "NOAA Ocean Service Education. Tides and Water Levels.," 2017. [Online]. Available: https://oceanservice.noaa.gov/education/kits/tides/tides08_othereffects.html. [Accessed: 11-Jan-2018].

[11]   J. Chavarría V., "Estudio comparativo de los niveles y fases de las mareas en el sistema Río Guayas-Estero Salado," Escuela Superior Politécnica del Litoral (ESPOL), 1988.

[12]   S. Murray, D. Conlon, A. Siripong, and J. Santoro, "Circulation and salinity

distribution in the Río Guayas Estuary, Ecuador," in *Geology and Engineering*, 1975, pp. 345–363.

[13]   E. Brown, A. Colling, D. Park, J. Phillips, D. Rothery, and J. Wright, *Ocean Circulation*, Second. Open University, Walton Hall, Milton Keynes MK7 6AA and Butterworth-Heinemann, 2001.

[14]   PRASDES CIIFEN, "Informe de evaluación de impactos del Fenómeno El Niño 2015 2016," 2016.

[15]   National Oceanic and Atmospheric Administration (NOAA), "NOAA National Weather Service. Climate Prediction Center." [Online]. Available: http://www.cpc.ncep.noaa.gov/data/indices/. [Accessed: 10-Jan-2018].

[16]   E. Cucalon, "Oceanographic variability off Ecuador associated with an El Niño event in 1982-1983," *J. Geophys. Res. Ocean.*, vol. 92, no. C13, pp. 14309–14322, 1987.

[17]   INAMHI, "Boletin Climatologico Anual 2015," 2016.

[18]   INAMHI, "BOLETÍN CLIMÁTICO MENSUAL DE GUAYAQUIL Y SUS ALREDEDORES. Boletín Mensual Año III- N°4," 2015.

[19]   INAMHI, "BOLETÍN METEOROLÓGICO DE GUAYAQUIL Y SUS ALREDEDORES. Boletín Año II- N° 108.," 2015.

[20]   INAMHI, "BOLETÍN METEOROLÓGICO DE GUAYAQUIL Y SUS ALREDEDORES. Boletín Año II- N° 115.," 2015.

[21]   INAMHI, "BOLETÍN CLIMÁTICO MENSUAL DE GUAYAQUIL Y SUS ALREDEDORES. Boletín Mensual Año III- N°6," 2015.

[22]   INAMHI, "BOLETÍN METEOROLÓGICO DE GUAYAQUIL Y SUS ALREDEDORES. Boletín Año II- N° 155.," 2015.

[23]   INAMHI, "BOLETÍN METEOROLÓGICO DE GUAYAQUIL Y SUS ALREDEDORES. Boletín Año II- N° 174.," 2015.

[24]   INAMHI, "BOLETÍN CLIMÁTICO MENSUAL DE GUAYAQUIL Y SUS ALREDEDORES. Boletín Mensual Año II- N° 4," 2014.

[25]   INAMHI, "Boletín Meteorológico de Guayaquil y sus alrredededores. Boletín Año II- N° 97," 2014.

[26]   INAMHI, "BOLETÍN METEOROLÓGICO DE GUAYAQUIL Y SUS ALREDEDORES. Boletín Año II- N° 119," 2014.

[27]   INAMHI, "BOLETÍN CLIMÁTICO MENSUAL DE GUAYAQUIL Y SUS ALREDEDORES. Boletín Mensual Año II- N°6," 2014.

[28] INAMHI, "BOLETÍN METEOROLÓGICO DE GUAYAQUIL Y SUS ALREDEDORES. Boletín Año II- N° 154," 2014.

[29] INAMHI, "BOLETÍN METEOROLÓGICO DE GUAYAQUIL Y SUS ALREDEDORES. Boletín Año II- N° 161," 2014.

[30] Deltares, "Delft3D Functional Specifications," Delft, 2016.

[31] Deltares, "Delft3D-FLOW. Simulation of multi-dimensional hydrodynamic flows and transport phenomena, including sediments. User Manual. Hydro-Morphodynamics," Delft, 2016.

[32] F. G. Bosch van Drakestein, "Modeling of tides and spreading of saline water in the Arabian Gulf and in the coastal area of Abu Dhabi with a flexible mesh model," Utretch University, 2014.

[33] Deltares, "RGFGRID. Generation and manipulation of structured and unstructured grids, suitable for Delft3D-FLOW, Delft3D-WAVE or D-Flow Flexible Mesh. User Manual," Delft, 2016.

[34] Deltares, "QUICKIN. Generation and manipulation of grid-related parameters such as bathymetry, initial conditions and roughness. User Manual," Delft, 2016.

[35] INOCAR, "Tabla de mareas y datos astronómicos del sol y de la luna," Guayaquil, Ecuador, 2015.

[36] J. J. van der Werf, "Hydrodynamic validation of Delft3D using data from the SandyDuck97 experiments," 2009.

[37] P. D. Barrera Crespo, "Delft3D Flexible Mesh modelling of the Guayas River and Estuary system in Ecuador," DelftUniversity of Technology, NationalUniversity of Singapore, 2016.

[38] IH CANTABRIA, "CONVIVE-LIFE. Deliverable Action A2. Estudio hidrodinámico de las actuaciones de restauración. Estuario de Oyambre."

[39] IH CANTABRIA, "Anexo VII. Documento 1. Estudio sobre la adaptación al cambio climático de la costa del principado de Asturias. Generación e integración de bases de datos climáticas y de vulnerabilidad," 2016.

[40] N. K. Ganju, M. J. Brush, B. Rashleigh, A. L. Aretxabaleta, P. del Barrio, J. S. Grear, L. A. Harris, S. J. Lake, G. McCardell, J. O'Donnell, D. K. Ralston, R. P. Signell, J. M. Testa, and J. M. P. Vaudrey, "Progress and Challenges in Coupled Hydrodynamic-Ecological Estuarine Modeling," *Estuaries and Coasts*, vol. 39, no. 2, pp. 311–332, 2015.

[41] X. Zhao, "NUMERICAL MODELLING OF MORPHOLOGICAL DEVELOPMENT IN A MANAGED REALIGNMEN T PROJECT. A case study of the Perkpolder project, Western Scheldt, The Netherlands," University of Twente, 2016.

[42] L. Velásquez Montoya, "Análisis de sensibilidad a un modelo de transporte de sedimentos: Golfo de Urabá, Colombia," Universidad EAFIT, 2011.

[43] INOCAR, "Calendario de aguajes y fase lunar 2018." [Online]. Available: http://www.inocar.mil.ec/web/index.php/productos/calendario-aguajes. [Accessed: 16-Nov-2017].

[44] D. E. Sánchez Marin, "Elaboración de un modelo hidrodinámico entre las boyas 27 y 59 del canal de acceso al Puerto Marítimo de Guayaquil utilizando el software DELFT3D," Escuela Superior Politécnica del Litoral, 2015.

[45] K. Kumbier, R. C. Carvalho, A. T. Vafeidis, and C. D. Woodroffe, "Investigating compound flooding in an estuary using hydrodynamic modelling: A case study from the Shoalhaven River, Australia," *Nat. Hazards Earth Syst. Sci. Discuss.*, no. October, pp. 1–28, 2017.

[46] P. Dissanayake, H. Karunarathna, and R. Ranasinghe, "Numerical modelling of the impact of sea level rise on large tidal inlet/basin systems," in *IAHR 2015: 36th IAHR World Congress: Deltas of the Future (and what happens upstream)*, 2015.

[47] L. T. Helaire, "Modeling of Historic Columbia River Flood Impacts Based on Delft 3D Simulations," Portland State University, 2016.

[48] A. Amenaghawon, "Tidal Influence on Epiphyton Population of Okpoka Creek, Upper Bonny Estuary, Nigeria Onome," *Int. J. Sci. Res. Knowl.*, vol. 1, no. 10, pp. 373–456, 2013.

[49] M. Valencia, L. Burgos, and M. E. de Espinoza, "Estudio en calidad de las aguas del Estero del Muerto en base a la concentración de oxígeno disuelto.- Estación fija.," *Acta Ocean. del Pacífico, INOCAR.*, vol. 4, no. 1, 1987.

[50] M. CÁRDENAS CALLE, "Efecto De La Contaminación Hidrocarburífera Sobre La Estructura Comunitaria De Macroinvertebrados Bentónicos Presentes En El Sedimento Del Estero Salado," p. 120, 2010.

[51] A. Rodriguez, "Contaminación por residuo de hidrocarburo del petroleo en

el Puerto Marítimo de Guayaquil y su área de influencia debido a actividades navieras, período 1984-2004," *Acta Ocean. del Pacífico*, vol. 103, no. 1, pp. 2005–2006, 2005.

[52] Z. Yang, T. Khangaonkar, and S. Breithaupt, "Modeling of tidal circulation and pollutant transport in Port Angeles Harbor and Strait of Juan de Fuca," *Proc. Int. Conf. Estuar. Coast. Model.*, no. September, 2004.

[53] J. G. Nath Nieto, "Características físicas y cálculo del prisma de marea en el Estero Cobina," Escuela Superior Politécnica del Litoral (ESPOL), 1993.